Pergamon

Geochimica et Cosmochimica Acta, Vol. 67, No. 13, pp. 2377–2395, 2003

0016-7037/03 $30.00 + .00

doi:10.1016/S0016-7037(03)00022-X

Control of ^{36}Cl production in carbonaceous shales by phosphate minerals

GREGORY CHMIEL,[1,*] STEVEN J. FRITZ,[1] and DAVID ELMORE[2]

[1]Department of Earth & Atmospheric Sciences, Purdue University, West Lafayette, IN 47907, USA
[2]Department of Physics, Purdue University, West Lafayette, IN 47907, USA

(*Received May* 22, 2001; *accepted in revised form December* 9, 2002)

Abstract—When using ^{36}Cl to date very old groundwater in regional aquifer systems, knowledge of the subsurface ^{36}Cl input into the aquifer system is essential. Although ^{36}Cl can be produced through nuclear reactions in the subsurface, in many situations, the input of ^{36}Cl into sedimentary aquifer systems by this avenue of production can be neglected. This is a valid assumption when investigating long-flowpath groundwater systems composed of sandstones, limestones, and shales of typical composition. These rock types are not sufficiently enriched in radioactive elements to produce significant ^{36}Cl in the deep subsurface. Carbonaceous shales, on the other hand, can concentrate the radioactive elements necessary to produce significant ^{36}Cl in the deep subsurface. Chlorine-36 ratios (^{36}Cl/Cl) for a suite of Late Devonian and Pennsylvanian carbonaceous shales were calculated from bulk-rock chemistry as well as measured using accelerator mass spectrometry. The poor agreement between calculated and measured ratios is the result of the assumption of chemical homogeneity used by the calculation algorithm, an assumption that was not satisfied by the carbonaceous shales. In these shales, organic matter, clay minerals, and accessory minerals are heterogeneously distributed and are physically distinct on a micron-order scale. Although organic matter and clay minerals constitute the overwhelming bulk of the shales, it is the phosphate minerals that are most important in enhancing, and suppressing, ^{36}Cl production. Minerals such as apatite and carbonate-apatite (francolite)—by including uranium, rare earth elements (REEs), and halogens—have an important impact on both neutron production and thermal neutron absorption. By incorporating both uranium and fluorine, phosphate minerals act as neutron production centers in the shale, increasing the probability of ^{36}Cl production. By incorporating REEs and chlorine, phosphate minerals also act to shield ^{35}Cl from the thermal neutron flux, effectively suppressing the production of ^{36}Cl. To reconcile the measured ^{36}Cl ratios with the ratios calculated assuming chemical homogeneity, the shales were artificially split into three fractions: organic, clay mineral, and phosphate mineral. Neutron production was calculated separately for each fraction, and the calculation results demonstrated that the phosphate fraction exerted much more control on the ^{36}Cl ratio than the organic or clay mineral fractions. By varying the uranium and chlorine contents in the phosphate fraction, a new, heterogeneous ^{36}Cl ratio was calculated that agreed with the measured ratio for the overwhelming majority of the carbonaceous shales. When using rock chemistry to calculate the ^{36}Cl ratio, rock types that show mineralogical heterogeneity on a micron scale can be divided into bulk fractions and accessory fractions for separate calculations of neutron production and neutron absorption. In this manner, a more accurate, heterogeneous ^{36}Cl ratio can be calculated for the rock as a whole.

1. INTRODUCTION

Groundwater age dating has achieved new importance in recent years for scientific as well as public policy reasons. The pressing need to store radioactive waste has initiated projects such as the International Stripa Project (cf. *Geochimica et Cosmochimica Acta*, vol. 53, no. 8) and the Yucca Mountain Project, both aimed at determining groundwater flow patterns and groundwater ages for the purpose of studying the effects of long-term radioactive waste storage. Of the three important cosmogenic nuclides (^{3}H, ^{14}C, and ^{36}Cl) used for groundwater dating, only ^{36}Cl is truly useful for very old groundwaters (Bentley et al., 1986). This isotope has two important characteristics that give it additional advantages in groundwater dating. One is the relatively long half-life of 3.01×10^5 yr (Parrington et al., 1996), which provides an ultimate dating range from 5 to 7 half-lives, or 1.5 million to ~2 million yr (Lehmann et al., 1990; Nolte et al., 1991), though subsurface input of chlorine from aquifer-formation rock can lower these limits (Phillips, 2000). The second advantage ^{36}Cl enjoys is that this isotope exists in water as the chloride ion. The chemical conservativeness of chloride ensures that it is not involved in oxidation-reduction reactions and also is not subject to biologic fixation. In addition, considering the mass of the isotopes, chloride ions are expected to experience little or no isotopic fractionation over the course of a long-flow aquifer system.

The majority of natural ^{36}Cl that is active in the hydrologic cycle is produced in the atmosphere by spallation reactions involving cosmic ray interactions with argon (Bentley et al., 1986). In the subsurface, measurable ^{36}Cl is created through neutron activation of stable ^{35}Cl, where neutrons are produced from spontaneous fission of ^{238}U as well as from the interactions of α particles with light nuclei of atoms such as aluminum, sodium, and magnesium—the (α,n) reaction (Feige et al., 1968). Alpha particles are generated by nuclei in the long-lived decay chains of ^{238}U, ^{235}U, and ^{232}Th. Subsurface production of ^{36}Cl via neutron activation is typically not an important contributor to the total ^{36}Cl content of sedimentary aquifer

* Author to whom correspondence should be addressed (gjc@expert.ics.purdue.edu).

systems; the common sedimentary rock types (such as sandstone, siltstone, limestone, and shale) do not contain sufficient uranium and thorium to produce enough ^{36}Cl to rival the spallation-produced ^{36}Cl in infiltrating precipitation. This is especially true when these rock types are viewed with respect to their average composition (cf. Table 3 in Fabryka-Martin et al., 1987). Carbonaceous shales, however, are quite different from shales of average composition.

Shales that contain $>$ 2% organic carbon are classified as carbonaceous or black shales (Tourtelot, 1979). Carbonaceous shales are an important subgroup of shales; they make their first appearance in the Proterozoic and are found in all periods of the Paleozoic, Mesozoic, and Cenozoic (Tourtelot, 1979). Periods during which black shales achieved significant areal extent include the Silurian, Upper Devonian, Pennsylvanian, Upper Jurassic, and the Middle Cretaceous (Klemme and Ulmishek, 1991). Carbonaceous shales are different, with respect to ^{36}Cl production, from shales of average composition because of their ability to concentrate uranium. The affinity between uranium and organic matter has been known for some while (Moore, 1954; Szalay, 1964). During deposition at standard temperatures, organic matter that contains carboxylic acid functional groups forms stable organometallic complexes with soluble uranium (Meunier et al., 1990). During thermal maturation of the carbonaceous sediment, the uranyl-organic complex becomes unstable, and the reduction of U(VI) to U(IV) in uraninite is favored (Nakashima et al., 1984; Meunier et al., 1990). The uranium-organic complex is favored only in slightly acidic waters, and uranium-carbonate complexes are more important in neutral and alkaline waters (Shanbhag and Choppin, 1981). Fisher and Wignall (2001), in their study of an Upper Carboniferous black shale, found that although a positive correlation existed between uranium and organic carbon, uranium was primarily included in francolite, a carbonate-apatite. In this case, the highest uranium concentrations were not associated with beds representing the most persistent anoxic intervals; rather, the highest uranium concentrations were found in the transitions between facies, transitions that were characterized by fluctuating redox conditions during deposition. These fluctuating redox conditions favored the release of organic phosphorous and the subsequent formation of authigenic francolite, providing a mineralogical sink for uranium (Fisher and Wignall, 2001). The redistribution of uranium from organic complexes to the mineral francolite did not mask the control over uranium that organic matter exercised during deposition and thus did not change the positive correlation between organic carbon and uranium in that study.

Carbonaceous shales can concentrate significant uranium. A survey of Late Devonian age carbonaceous shale found uranium contents of 36 ppm in West Virginia, 77 ppm in Tennessee, 89 ppm in Kentucky, and 179 ppm in Indiana (Leventhal and Kepferle, 1982), much higher than the 3.2 ppm uranium of the "average" shale as reported by Vinogradov (1962). Although this is a simplification, ^{36}Cl ratios that are calculated on the basis of chemical composition can be viewed in proportion to uranium content. Thus, if a shale has a uranium content of 4.5 ppm and a calculated ^{36}Cl ratio ($^{36}Cl/Cl$) of 12.5×10^{-15} (Bentley et al., 1986), then a simple proportional calculation using the uranium concentrations listed above (for Late Devonian shales) would indicate a range of ^{36}Cl ratios of 100×10^{-15} to 500×10^{-15} for those carbonaceous shales. These ratios are similar to the ^{36}Cl rainwater ratio of 45×10^{-15} at Stripa, Sweden (Andrews et al., 1989); the recharge water ratio of 500×10^{-15} for the Milk River Aquifer, Alberta, Canada (Phillips et al., 1986); and the average rainwater ratio of 700×10^{-15} for north central Indiana (Vogt et al., 1994).

Subsurface input of ^{36}Cl cannot be neglected in the determination of groundwater age if the groundwater has significant contact with rock types—such as carbonaceous shales—that can maintain a ^{36}Cl ratio similar to that of the infiltrating water. In these cases, it is very important to have reliable chemistry and mineralogical distribution data on the rock that is contributing the ^{36}Cl. Not only did the carbonaceous shales studied for this project produce significant ^{36}Cl, but the algorithm used to calculate the ^{36}Cl ratios for these shales was in error more often than it was correct. The alterations made to the calculation algorithm are meant to reconcile the differing calculated and measured ^{36}Cl ratios and are based on the recognition that certain elemental associations can have a very important effect on ^{36}Cl production. This is especially true for accessory minerals that can host elements in very high concentrations.

2. EXPERIMENTAL METHODS

2.1. Collection of Shale Samples

The carbonaceous shale samples were of two different types, all collected in Indiana. Eleven samples represent Late Devonian shales belonging to the New Albany Shale formation. These shales were deposited in a marine environment and the organic material is dominated by type II kerogen (Hover et al., 1996) primarily composed of autochthonous organic matter but also including phyto- and zooplanktonic remains (Tissot and Welte, 1978). Ten of these shale samples were acquired from the Indiana Geological Survey core library, and 1 was a grab sample from an outcrop in Carroll County, Indiana. The remaining 5 shale samples are Pennsylvanian, deposited in a near-shore environment in association with coal swamps; the organic material is dominated by type III kerogen composed primarily of terrestrial vascular plants (Breger et al., 1983). Three of the Pennsylvanian samples were taken from the Viking Coal Mine, Daviess County, Indiana. These shales belong to the Lower Pennsylvanian Raccoon Creek Group (Gray et al., 1987; Friedman, 1989). The other 2 Pennsylvanian samples were taken from the Columbia Coal Mine, Gibson and Pike Counties, Indiana. These shales belong to the Middle Pennsylvanian Carbondale Group (Gray et al., 1987; Friedman, 1989).

2.2. Extraction of Chloride From the Shale Samples

Chlorine-36 ratio measurements were performed at the Purdue Rare Isotope Measurement Laboratory (PRIME Lab). This facility requires a target material of silver chloride for measuring the ^{36}Cl ratio by accelerator mass spectrometry (AMS). The target was prepared by extracting chlorine from powdered shale through oxidation in an aqueous medium and then isolating, purifying, and precipitating the chlorine as silver chloride.

The use of an oxidant to extract chlorine from the shales was based on the positive correlation between chlorine and carbon ($r^2 = 0.72$ for the 11 New Albany Shale samples and $r^2 = 0.78$ for the five Pennsylvanian shale samples). A 30% hydrogen peroxide (H_2O_2) solution was used to consume the organic matter and liberate chloride, which would have been released into solution as HCl. Further oxidation beyond what was needed to liberate chloride from organic matter could oxidize Cl^- to Cl^0, possibly forming chlorine gas that could be lost by volatilization. The equation is

$$2H^+ + 2Cl^- + H_2O_2 \leftrightarrow Cl_{2(aq)} + 2H_2O. \quad (1)$$

At 25°C,

$$K_{eq} = 10^{14.9} = \frac{[Cl_{2(aq)}][H_2O]^2}{[H^+]^2[Cl^-]^2[H_2O_2]}. \quad (2)$$

For the sake of simplicity, all activity coefficients are assumed to be unity such that the activity of each species is equal to the molarity of each species. Assigning H_2O_2 an activity of 0.3 because of its 30% concentration, the minimum $[H^+]$ necessary for Eqn. 1 to proceed is

$$[H^+]_{min} = \frac{10^{-7.2}\sqrt{Cl_{2(aq)}}}{[Cl^-]}. \quad (3)$$

The mass balance for chlorine in Eqn. 1 can be written as $Cl_T = [Cl^-] + 2[Cl_{2(aq)}]$. The total chlorine content (Cl_T) is assumed to be the chlorine leached out of the shale. By varying the pH and by assuming a reasonable total chlorine content for the solution such as 10 to 20 ppm, either $[Cl^-]$ or $[Cl_{2(aq)}]$ can be solved numerically. If the pH were kept above 6 during the oxidation process, then the $[Cl^-]/[Cl_{2(aq)}]$ ratio would have been > 100, and it is a safe assumption that chlorine would have remained in solution as the chloride ion. However, even if the pH were in the range of 4 to 5 during the oxidation process—which is a more reasonable estimate—carbon, sulfur, and iron would be preferentially oxidized in these shales before the -1 valence of chloride would be altered. The half-cell voltages of these three elements' oxidation reactions are much less positive than that of chlorine (Krauskopf, 1979), and all the shale samples have carbon, sulfur, and iron concentrations well in excess of the chlorine concentration (see Table 1). Thus, we believe that little or no chlorine would have been lost because of volatilization during the oxidation of the shale powder.

The process of extracting chlorine from the shales is detailed in Chmiel (1999). Chips of shale were reduced in size using a jaw crusher and subsequently powdered in a shatterbox. The shale powder, which passed a 106-μm sieve, was slurried with deionized water and oxidized with a 30% hydrogen peroxide solution. The usual mass-to-mass ratio of peroxide to shale powder was 10:1, resulting in 100 g of shale (slurried in 250 g of deionized water) being oxidized with 1000 g of hydrogen peroxide solution. The hydrogen peroxide solution was added in 10- to 20-g aliquots. These shales contained a significant quantity of sulfur as pyrite, which upon oxidation formed sulfuric acid. Because the oxidation reaction proceeded more favorably in a neutral-pH medium, $\sim$5 mL of concentrated ammonium hydroxide were added throughout the oxidation process to neutralize the presence of sulfuric acid. After the addition of the hydrogen peroxide solution was complete, the slurry was heated to reduce the total volume to $\sim$500 mL. The residual shale powder was removed by filtration, and the pH of the filtrate was adjusted to near neutral through the addition of concentrated ammonium hydroxide. The resulting iron hydroxide precipitate was oxidized using 10 to 20 g of 30% hydrogen peroxide solution and removed by filtration. The solution was heated (5 h on average) to reduce the volume, and iron hydroxide and in some cases calcium sulfate were removed by filtration. A second round of heating (2 h on average) and filtration was also performed. These heatings and filtrations were necessary to remove as much iron hydroxide from the solution as necessary. Tests performed before working with the actual shale samples showed that if iron hydroxides were still present during the purification process, they would precipitate on the anion exchange beads. As a final step to remove sulfate, 20 drops of a 3% barium nitrate solution were added to the solution, and the resulting barium sulfate was removed by filtration. The solution was acidified with 12.5 mL of concentrated nitric acid, on average, and silver chloride was precipitated upon the addition of an average of 15 drops of high-purity 1-mol/L silver nitrate solution. This silver chloride was washed with deionized water, placed back into solution using 5 mL of concentrated ammonium hydroxide, and reprecipitated upon the addition of 7.5 mL of concentrated nitric acid. Centrifugation of this suspension provided the final isolation of the silver chloride.

The chloride was then purified by means of simple chromatography following a method supplied by the PRIME Lab chemistry operations. The isolated silver chloride (in 5 mL of deionized water) was dissolved using 20 to 30 drops of concentrated ammonium hydroxide and poured into an exchange column (of 1 cm in diameter) containing 5 cm height of nitrate-loaded anion exchange beads. The centrifuge tube was rinsed first with 10 mL of 0.01-mol/L ammonium hydroxide, which was poured into the column, followed by a rinse of 10 mL of 0.05-mol/L nitric acid, which was also poured into the column. The chloride was moved down the column using 5 mL of 0.15-mol/L nitric acid, and the subsequent additions of 2 mL of 0.15-mol/L nitric acid and 15 mL of 0.15-mol/L nitric acid to the column were collected in a centrifuge tube containing 3 drops of 1–mol/L silver nitrate. Three more drops of 1-mol/L silver nitrate were added to the centrifuge tube as well as 5 drops of concentrated nitric acid. The silver chloride precipitate was centrifuged, washed with deionized water, and dried at 60°C. The ^{36}Cl ratio was measured on the purified silver chloride target at PRIME Lab by AMS. Details of this procedure can be found in Purser et al. (1994).

Reagent-grade ammonium chloride was subjected to the same procedures as the shale samples, and the ^{36}Cl ratio was measured for use as a chemistry blank. As can be seen from Table 2, the ^{36}Cl ratio of this blank was high ($23.9 \pm 3.3 \times 10^{-15}$). Thus, all solutions that were added in significant quantities during the chemistry procedure were tested for ^{36}Cl. For the hydrogen peroxide test, 500 g of 30% hydrogen peroxide and 2.5 mL of concentrated nitric acid were added to a solution of 16 mg of ammonium chloride in 68 mL of deionized water. The ^{36}Cl ratio of the chloride precipitated from this solution after the addition of 10 drops of 1-mol/L silver nitrate was $2.0 \pm 4.9 \times 10^{-15}$. For the nitric acid test, 20 mL of concentrated nitric acid were added to a solution of 16 mg of ammonium chloride in 40 mL of deionized water. The ^{36}Cl ratio of the chloride precipitated from this solution after the addition of 10 drops of 1–mol/L silver nitrate was $0 \pm 2.9 \times 10^{-15}$. For the ammonium hydroxide test, 25 mL of concentrated ammonium hydroxide and 20 mL of concentrated nitric acid were added to a solution of 16 mg of ammonium chloride in 37 mL of deionized water. The ^{36}Cl ratio of the chloride precipitated from this solution after the addition of 10 drops of 1-mol/L silver nitrate was $0 \pm 4.6 \times 10^{-15}$. In addition, the chloride separation and purification procedure was tested by taking up 16 mg of ammonium chloride into solution with concentrated ammonium hydroxide and passing the solution through an ion exchange column. This sample was subjected to the procedure outlined above for moving and collecting the chloride off the exchange beads. The ^{36}Cl ratio of the chloride precipitated from this solution after the addition 2.5 mL of concentrated nitric acid and 10 drops of 1-mol/L silver nitrate was $0.5 \pm 2.3 \times 10^{-15}$. Because it did not appear that the reagents were causing the high value of the chemistry blank, ^{36}Cl addition due to fallout from the air was tested. For the open system test, 20 mg of ammonium chloride and 9 drops of 1-mol/L silver nitrate were added to 100 mL of deionized water in a 1-L beaker having an approximate area open to the atmosphere of 78.5 cm^2. The beaker was left open for 60 h. For the closed system test, 21 mg of ammonium chloride and 9 drops of 1-mol/L silver nitrate were added to 100 mL of deionized water in an Erlenmeyer flask. This flask was closed off from the atmosphere for 60 h. Upon termination of the experiment, 3 drops of concentrated nitric acid were added to both solutions to aid in the precipitation of silver chloride. The silver chloride was mechanically separated from the solution and submitted for ^{36}Cl ratio measurement. The ^{36}Cl ratio for the open system was $17 \pm 11 \times 10^{-15}$, and the ratio for the closed system was $0.1 \pm 3.5 \times 10^{-15}$. Atmospheric contamination appears to be the primary culprit for the high ^{36}Cl ratio of the chemistry blank, even though exposure to the atmosphere during processing was minimized. Because none of the shale samples received treatment that was significantly different from the others, especially with respect to being open to the atmosphere, it was assumed that the chemistry blank was a true representation of the background ^{36}Cl added during the process. Thus, although the ratio was high, all the measurements for the shale samples were adjusted downwards using this ratio.

2.3. Chemical Analyses of the Shales

The ^{36}Cl ratio of a rock can be calculated through knowledge of the bulk-rock chemistry. To compare the measured ^{36}Cl ratios of these shales to calculated ratios, shale samples (as splits from the same powders that were oxidized to extract ^{36}Cl for AMS) were sent to XRAL Laboratories, Don Mills, Ontario, Canada, for chemical analysis. The results of these analyses are presented in Table 1. The major oxides (SiO_2, Al_2O_3, CaO, MgO, Na_2O, K_2O, Fe_2O_3, MnO, Cr_2O_3, P_2O_5, and TiO_2) were determined using X-ray fluorescence. Fluorine and chlorine were determined by specific ion electrode after sample digestion using Na_2O_2 (sodium peroxide) fusion. Carbon, sulfur, and structural water (H_2O^+) were determined by infrared combustion.

Table 1. Elemental composition of the shales. All concentrations are in parts per million unless otherwise noted. The naming scheme for the New Albany Shales consists of the Indiana Geological Survey core library identification number followed by the name of the Indiana county from which the sample was collected. The Carroll sample was taken from an outcrop in Carroll County, Indiana. The Pennsylvanian shales are named for their coal mine of origin and the sequential order in which they were taken.

Sample	Si	Al	Ca	Mg	Na	K	Fe	Mn	Ti	P	Cr	C	S	H_2O^+ (%)
New Albany Shales														
6 Vigo	210,000	63,000	66,000	17,100	2600	35,600	44,600	200	3570	680	100	101,000	36,500	3.60
187 Antrim	271,000	59,300	8510	13,400	3000	34,700	44,700	200	3770	300	70	75,300	30,300	3.90
187 Ellsworth	267,000	70,400	23,700	23,100	3300	42,100	36,900	300	4470	200	100	37,500	10,400	3.00
428 Harrison	240,000	61,900	1400	8500	2200	37,900	62,800	200	4480	560	100	124,000	48,300	3.60
432 Harrison	245,000	74,100	3400	10,700	1600	41,700	46,100	200	4630	1200	100	109,000	24,200	3.40
611 Harrison	245,000	65,100	10,900	8800	1200	35,400	39,200	200	4560	3600	200	134,000	23,000	3.20
507 Putnam	249,000	75,700	1400	11,200	2400	41,700	45,500	200	4920	400	100	84,300	24,400	5.10
554 Sullivan	250,000	74,100	4800	10,900	2500	39,700	33,500	200	4680	1100	300	130,000	11,000	3.30
628 Morgan	220,000	63,500	3100	9710	70	36,300	36,700	200	4300	1100	600	180,000	19,500	4.00
634 Morgan	215,000	64,000	2400	10,000	<70	36,700	36,400	200	4390	850	680	197,000	21,800	4.40
Carroll	257,000	67,700	10,100	14,300	2300	33,900	47,800	300	4500	500	100	91,200	29,400	4.70
Pennsylvanian shales														
Viking A	267,000	112,000	4400	10,300	1300	33,100	38,000	500	5560	960	100	11,700	3700	5.40
Viking B	127,000	52,100	8720	7300	<70	19,800	42,300	200	3830	1900	600	381,000	25,200	3.20
Viking D	236,000	91,000	7930	10,900	3100	28,800	42,500	200	5490	1200	400	79,300	23,800	5.10
Columbia E	144,000	61,400	16,700	11,000	1200	25,700	39,400	200	3600	2600	890	299,000	22,700	3.30
Columbia F	162,000	68,800	15,400	11,000	3200	27,600	40,900	200	4120	3300	820	244,000	24,800	3.90
Average shale[a]	238,000	104,500	25,300	13,400	6600	22,800	33,300	670	4500	770	100	10,000	3000	NA[b]

[a] Shale of average composition as compiled by Vinogradov (1962).
[b] NA denotes not included in this compilation.

Included water (H_2O^-) was determined gravimetrically. Boron, beryllium, and lithium were determined by inductively coupled plasma optical emission spectroscopy after Na_2O_2 fusion. Thorium, uranium, and the rare earth elements (REEs) were determined by inductively coupled plasma mass spectroscopy after Na_2O_2 fusion.

2.4. Gamma Spectrometry Determination of ^{226}Ra in the Shales

A simplifying assumption in the calculation of the ^{36}Cl ratio is that all nuclides in the three naturally occurring decay chains are in secular equilibrium. To test whether nuclides in the ^{238}U chain may have been lost subsequent to initial ^{238}U decay, ^{226}Ra activities were determined in the shales by γ-ray spectrometry. The procedure is detailed in Gladney et al. (1991). Samples of the same shale powder used for the AMS measurement and chemical analysis were sealed in metal canisters for 35 d until ^{214}Bi ($t_{1/2}$ = 19.9 min) and ^{214}Pb ($t_{1/2}$ = 27 min) reached secular equilibrium with ^{226}Ra ($t_{1/2}$ = 1599 yr). The 186.2-keV γ of ^{226}Ra has a weak yield and is close to the 185.7-keV γ of ^{235}U. Thus, the strong signals of ^{214}Bi's 609.3-keV γ and ^{214}Pb's 351.9-keV γ were counted instead. The γ-ray spectrometer consisted of a liquid

Table 2. Measured ^{36}Cl ratios and adjustments to the ratios.

Sample	Depth below ground (m)	Measured ^{36}Cl/Cl ($\times 10^{-15}$)	Calculated cosmogenic component[a] ($\times 10^{-15}$)	Adjusted measured ^{36}Cl/Cl ($\times 10^{-15}$)
New Albany Shales				
6 Vigo	583	85.0 ± 4.4		61.1 ± 5.5
187 Antrim	72	80 ± 9		56.1 ± 9.6
187 Ellsworth	66	178 ± 8		154 ± 9
428 Harrison	241	44.9 ± 3.3		21.0 ± 4.7
432 Harrison	257	42.8 ± 5.2		18.9 ± 6.2
611 Harrison	70	49.2 ± 4.6		25.3 ± 5.7
507 Putnam	245	158 ± 6		134 ± 7
554 Sullivan	763	28.2 ± 3.5		4.3 ± 4.8
628 Morgan	154	29.0 ± 5.4		5.1 ± 6.3
634 Morgan	148	29.9 ± 4.5		6.0 ± 5.6
Carroll	2	312 ± 15	8.4	280 ± 15
Pennsylvanian shales				
Viking A	11	1602 ± 58	17.6	1561 ± 58
Viking B	12	332 ± 14	15.0	293 ± 14
Viking D	12	520 ± 24	14.9	481 ± 24
Columbia E	35	322 ± 25	2.6	296 ± 25
Columbia F	30	335 ± 14	3.2	308 ± 14
Chemistry blank		23.9 ± 3.3		

[a] A cosmogenic component to the ratio was not calculated for the cored New Albany Shale samples because they originated at depths at which the influence of cosmogenic production of ^{36}Cl on the total ratio is negligible.

H_2O^- (%)	Total H	Li	Be	B	F	Cl	Y	La	Ce	Pr	Nd	Sm	Eu	Gd	Tb	Dy	Ho	Er	Tm	Yb	Lu	Th	U
1.00	5150	26	3.8	166	1460	325	20	23.5	44.8	5.8	25.4	5.7	0.97	5.0	0.6	3.9	0.73	2.1	0.3	2.0	0.29	7.9	12.7
1.30	5820	30	3.6	119	869	597	21	23.4	48.3	5.6	23.2	5.3	0.89	4.7	0.6	4.0	0.81	2.4	0.3	2.3	0.33	7.1	28.4
1.60	5150	39	3.4	152	1050	337	21	28.2	60.8	6.6	26.1	5.6	0.93	4.8	0.7	4.1	0.78	2.4	0.3	2.3	0.35	9.7	9.0
1.00	5150	28	3.9	106	778	741	24	34.5	63.7	8.2	33.1	7.2	1.24	6.4	0.9	5.9	1.20	3.5	0.5	3.2	0.44	8.6	54.5
1.30	5270	42	3.9	136	1070	819	24	28.4	59.4	8.1	32.7	7.1	1.18	6.6	0.9	5.6	1.15	3.4	0.5	3.3	0.45	9.1	45.2
1.20	4920	29	3.3	120	1340	748	63	42.8	68.5	12.0	55.0	13.8	2.3	13.1	1.8	10.5	2.0	5.7	0.7	4.5	0.63	8.7	39.1
1.90	7840	40	4.2	158	937	266	26	31.1	59.4	7.2	28.5	6.0	0.95	5.3	0.7	4.5	0.95	2.9	0.4	2.7	0.37	9.8	37.5
1.00	4810	36	3.7	145	1160	776	41	35.7	55.9	8.1	34.9	7.7	1.28	7.3	1.0	6.1	1.27	4.0	0.5	3.7	0.56	8.2	23.4
2.00	6720	24	3.7	151	1070	1170	28	26.7	47.0	6.8	28.5	6.3	1.09	5.8	0.8	5.0	1.00	3.0	0.4	2.8	0.40	8.1	34.0
1.80	6930	25	3.3	139	949	1170	22	22.9	41.4	5.7	23.5	5.4	0.83	4.8	0.6	4.3	0.83	2.5	0.4	2.4	0.35	7.3	34.7
1.30	6720	27	4.1	117	1050	161	27	29.1	59.1	6.7	28.4	6.4	1.11	5.8	0.8	5.0	1.01	3.0	0.4	2.8	0.41	8.2	33.7
1.30	7500	76	4.5	97	1060	51	33	45.3	96.1	11.1	44.4	9.6	1.58	8.4	1.1	6.8	1.33	4.1	0.6	3.8	0.52	13.6	3.7
2.30	6150	21	3.7	69	1080	402	26	27.7	44.1	7.0	29.7	6.7	1.16	5.9	0.8	4.4	0.87	2.6	0.3	2.2	0.32	6.1	133
2.70	8730	36	5.5	119	1200	77	32	44.9	72.2	8.8	34.9	7.0	1.19	6.1	0.8	5.0	1.03	3.4	0.5	3.6	0.54	11.7	56.0
2.50	6490	16	3.6	76	1160	173	26	24.9	48.0	6.0	25.8	6.0	1.04	5.4	0.7	4.3	0.86	2.5	0.3	2.2	0.30	6.8	61.4
2.50	7160	25	4.6	88	1350	159	43	34.1	65.9	8.5	37.1	8.6	1.62	8.4	1.1	6.9	1.38	4.0	0.5	3.4	0.47	8.1	73.7
NA[b]	NA[b]	60	3	100	500	160	30	40	50	5	23	6.5	1	6.5	0.9	4.5	1	2.5	0.25	3	0.7	11	3.2

nitrogen cooled, high-purity germanium crystal (52.8 mm in diameter) shielded in a 10-cm-thick lead cavity.

2.5. Elemental Map Generation by Electron Microprobe

The elemental maps were constructed using the Viking B shale; backscattered images are shown in Figure 1, and the actual elemental maps are shown in Figure 2. The maps were made on an epoxy-mounted, carbon-coated, polished chip of the shale using a Cameca SX50 electron microprobe. The elemental map area (as shown in Figs. 1b and 2) is covered by 512 $\times$ 384 pixels (246 $\times$ 185 μm), and the microprobe, operating at 20 kV and 20 nA, received counts for a duration of 100 ms/pixel. The analyzing crystal for the silicon and potassium Kα wavelengths was pentaerithritol. For the aluminum and magnesium Kα wavelengths, the analyzing crystal was thallium acid pthalate. The analyzing crystal for the carbon and oxygen Kα wavelengths was the Ni/C multilayer pseudocrystal PC2 (Bustin et al., 1993).

3. RESULTS

3.1. Comparison of Calculated and Measured ^{36}Cl Ratios

Table 2 presents the ^{36}Cl ratios as measured by AMS. The raw measured ^{36}Cl ratios were adjusted downward for both the ^{36}Cl ratio of the chemistry blank and the calculated cosmogenic ^{36}Cl component for samples that were not taken from cores. Core samples were used for the majority of the shales to minimize the potential presence of cosmogenic ^{36}Cl. For the Carroll New Albany Shale sample and the Pennsylvanian samples, the cosmogenic ^{36}Cl component was calculated on the basis of shale composition and the depth below original ground surface. A full treatment of the cosmogenic ratio calculations performed on these shales is included in Chmiel (1999); the algorithm in that document was compiled from Zreda et al. (1991) for spallation-related production, Liu et al. (1994) for neutron-related production, Stone et al. (1998) for muon-related production, and references within those papers. Alternatively, the reader is referred to Gosse and Phillips (2001) for a complete treatment of cosmogenic ^{36}Cl production and to Phillips et al. (2001) for an improved approach to neutron-related ^{36}Cl production. The only sample sufficiently near to the ground surface to have measurable ^{36}Cl from cosmogenic neutron production was the Carroll New Albany Shale, collected at a depth of 2 m. The ^{36}Cl ratio due to cosmogenic neutron production (as calculated according to Liu et al., 1994) was 25% of the total calculated cosmogenic ratio for this shale, but only a minor 0.8% of the measured ^{36}Cl ratio for the shale less chemistry blank. The shallowest of the core samples, 187 Ellsworth, which was taken from a depth of 66 m below ground surface, had a calculated cosmogenic ^{36}Cl ratio of 3×10^{-17}. Thus, no cosmogenic calculations were performed on any of the other New Albany Shale samples taken from cores. The chemistry blank and cosmogenic subtractions make the adjusted measured ^{36}Cl ratio and the calculated ^{36}Cl ratio directly comparable; these quantities are presented in Table 3. Chlorine-36 ratios were calculated for these rocks using the algorithm presented in the Appendix. It should be noted that in addition to calculating the production of ^{36}Cl from the ^{35}Cl(n,γ)^{36}Cl and ^{39}K(n,α)^{36}Cl reactions, a calculation was performed to determine ^{36}Cl production from the ^{33}S(α,p)^{36}Cl reaction (Fabryka-Martin, 1988). Chlorine-36 produced from this process is minor, averaging 3% of the total calculated ratio for the New Albany Shale samples and 6% for the Pennsylvanian shales. The small contribution to the total calculated ratio lessens the importance of this process, and it will not be discussed further. The percent ratio difference between the calculated and measured ratios is a useful quantity to analyze trends in the ^{36}Cl ratios with respect to rock chemistry. It is calculated using

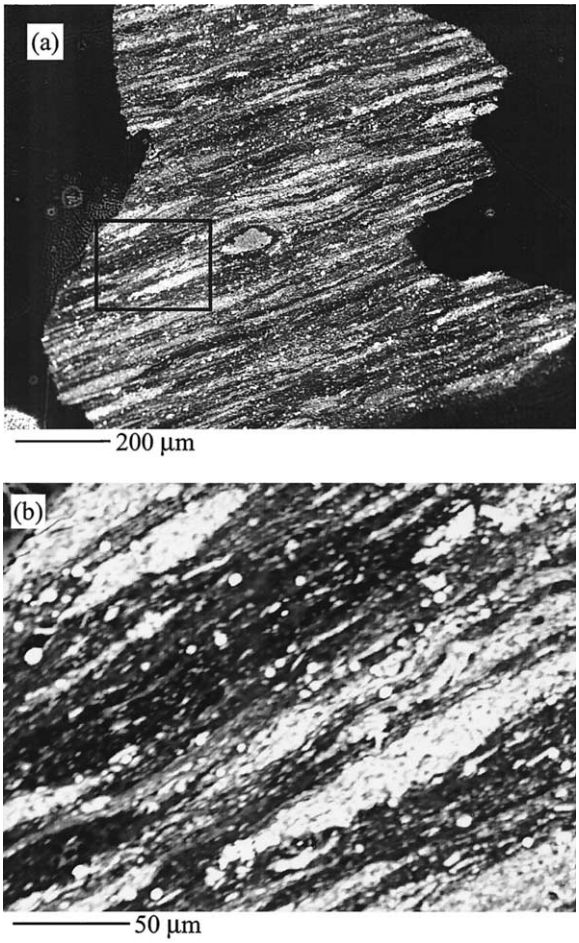

Fig. 1. (a) Backscattered image of the Viking B shale chip used for the elemental map. (b) Backscattered image of the area bound by the black rectangle in (a). This is the area used in the construction of the elemental maps in Figure 2.

$$\%\ \text{Ratio Difference} = \frac{\text{Adjusted Measured Ratio} - \text{Calculated Ratio}}{\text{Calculated Ratio}} \times 100\%. \quad (4)$$

As can be seen from Table 3, the majority of the measured ^{36}Cl ratios do not agree with calculated ratios. The average percent ratio difference, and thus the mean error in the calculation of the ^{36}Cl ratio, is +54% for the New Albany Shale samples, whereas for the Pennsylvanian shales, it is +98% (less the Viking A shale; see below). As a comparison, Phillips (2000, Fig. 10.6) presented a compendium of 36 samples for which the mean error in the calculation of the ^{36}Cl ratio is $< 3\%$. It should be noted that in the data set of Phillips (2000), 34 of the 36 samples are clustered in a reasonably tight group having measured and calculated ratios $< 60 \times 10^{-15}$. For the data presented in this paper, six of the seven shales that have measured ^{36}Cl ratios $> 100 \times 10^{-15}$ have measured ratios much higher than calculated, leading to a larger mean error relative to the data presented in Phillips (2000).

The Viking A sample has a very large measured ^{36}Cl ratio. This was the shallowest of the Pennsylvanian samples (taken at 11 m below ground surface), and it is assumed that this shale has been contaminated by bomb-pulse ^{36}Cl. The two other Viking samples were taken from a depth only 1 m below the Viking A sample. The Viking B and D samples, however, when combined with the Columbia samples, give rational results when comparing their percent ratio differences to carbon and magnesium (as shown in Fig. 3) as well as to elements such as aluminum, silicon, and total hydrogen (Chmiel, 1999). The relationships shown by the Pennsylvanian shales, with respect to percent ratio difference as a function of important elements, imitated the relationships shown by the New Albany Shale samples. The New Albany Shale samples are not expected to contain bomb-pulse ^{36}Cl contamination considering the depth below ground surface at which they were taken and their naturally low porosity. The only outcrop sample of the New Albany Shale is the Carroll sample, taken 2 m below ground surface. This sample, although it could be expected to show ^{36}Cl contamination because of its shallow depth, also graphs rationally with respect to the percent ratio difference and follows the trends set by the New Albany Shale data set as a whole. In hand sample, the Carroll shale could be mistaken for a slate; it is a very tight shale. On the basis of the above observations, it is assumed that the only shale in the sample set to have been contaminated by bomb-pulse ^{36}Cl contamination is the Viking A shale.

3.2. Assumptions for the Calculation of ^{36}Cl Ratios Using Bulk-Rock Chemistry

The production of ^{36}Cl can be viewed as occurring via a four-step sequence: (1) decay of an α-emitting nuclide, (2) nuclear reaction of the α particle with an appropriate nucleus to yield a neutron, (3) energy loss (i.e., thermalization) of the neutron through scattering interactions, and (4) capture of the thermal neutron by ^{35}Cl to form ^{36}Cl. In addition, it should be noted that ^{238}U does produce neutrons directly through spontaneous fission, effectively skipping to step 3. When calculating the ^{36}Cl ratio, it is common to assume that all nuclides in the three naturally occurring decay chains are in secular equilibrium. In these shales, neutron production due to uranium is an order of magnitude greater than thorium's for all but the low-uranium Viking A sample. Thus, if the ^{238}U decay chain were shown to be out of secular equilibrium, one would expect a difference between measured and calculated ^{36}Cl ratios. Because ^{238}U's decay chain includes long-lived isotopes such as ^{234}U ($t_{1/2} = 2.46 \times 10^5$ yr) and ^{230}Th ($t_{1/2} = 7.54 \times 10^4$ yr) before the formation of ^{226}Ra, and because the longest lived nuclide subsequent to ^{226}Ra is ^{210}Pb, with a half-life of 22.6 yr, the comparison of ^{238}U activity to ^{226}Ra activity is a valid benchmark for determining the extent of disequilibrium present in the ^{238}U decay chain. Assumed in this comparison is that because of the low porosity of these shales, radon will be retained during its short lifetime. Table 4 includes the results of the ^{226}Ra activity measurements. The excellent agreement between the calculated ^{238}U activities and the measured ^{226}Ra activities indicates that secular equilibrium exists between ^{238}U and its daughter nuclides for all the samples.

Returning to steps 2 through 4 in the ^{36}Cl production process, step 2 appears to be most likely affected by chemical

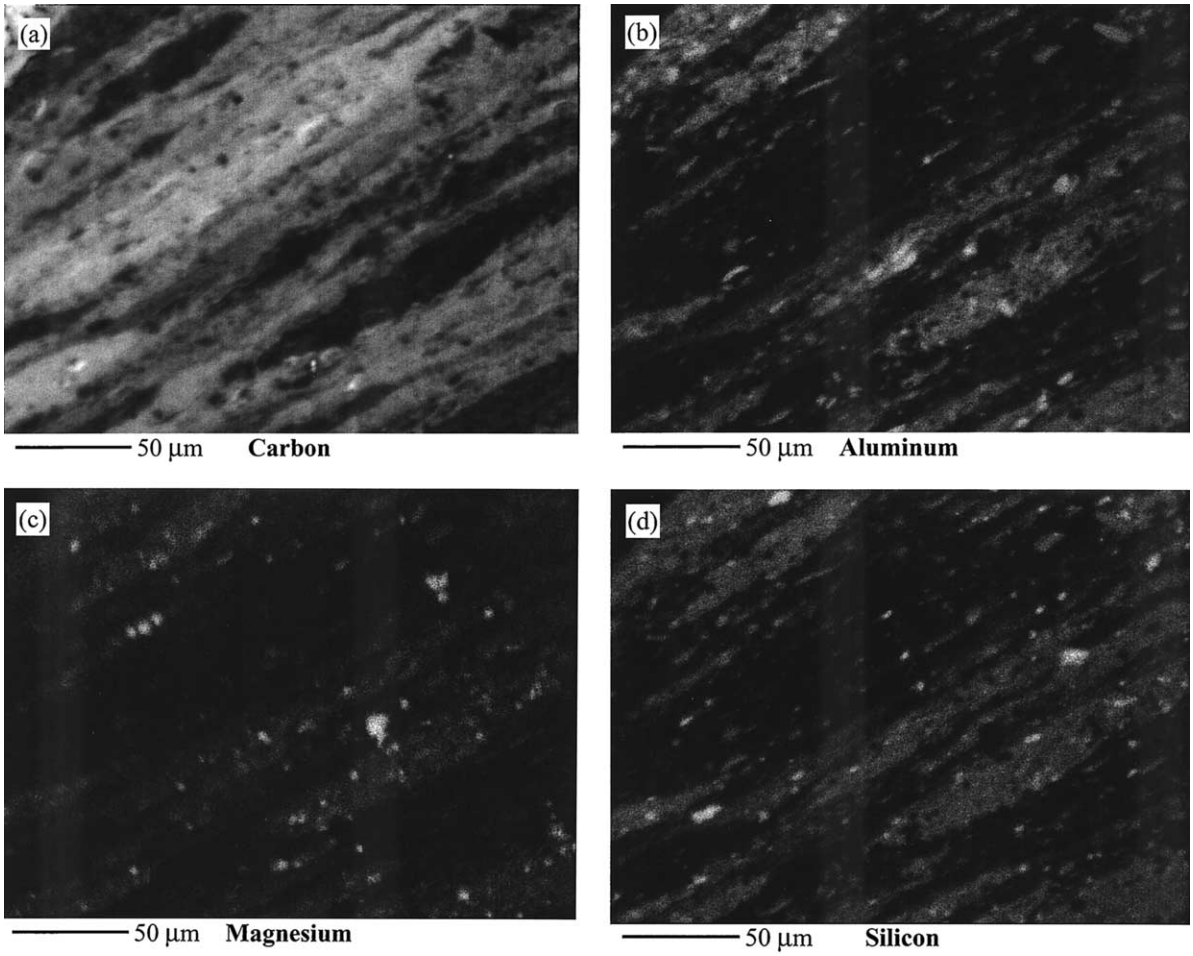

Fig. 2. All elemental maps correspond to the area shown in Figure 1b. In these plates, high concentrations of the element are white, grays represent intermediate concentrations, and black represents the absence of that element. (a) Elemental map of carbon. (b) Elemental map of aluminum. (c) Elemental map of magnesium. (d) Elemental map of silicon. Note that aluminum, silicon, and magnesium generally occupy areas of low or no carbon.

Table 3. Comparison of measured and calculated ^{36}Cl ratios.

Sample	C (%)	Cl (ppm)	U (ppm)	Th (ppm)	Adjusted measured ^{36}Cl/Cl ($\times 10^{-15}$)	Homogeneous calculated ^{36}Cl/Cl ($\times 10^{-15}$)	Percent ratio difference
New Albany Shales							
6 Vigo	10.1	325	12.7	7.9	61.1 ± 5.5	26.2 ± 1.9	+133 ± 24%
187 Antrim	7.53	597	28.4	7.1	56.1 ± 9.6	52.1 ± 4.2	+7.7 ± 20%
187 Ellsworth	3.75	337	9.0	9.7	154 ± 9	22.5 ± 1.7	+585 ± 59%
428 Harrison	12.4	741	54.5	8.6	21.0 ± 4.7	93.3 ± 7.2	−77 ± 11%
432 Harrison	10.9	819	45.2	9.1	18.9 ± 6.2	75.7 ± 6.2	−75 ± 13%
611 Harrison	13.4	748	39.1	8.7	25.3 ± 5.7	63.6 ± 5.0	−60 ± 13%
507 Putnam	8.43	266	37.5	9.8	134 ± 7	69.8 ± 5.1	+92 ± 14%
554 Sullivan	13.0	776	23.4	8.2	4.3 ± 4.8	41.5 ± 3.4	−90 ± 16%
628 Morgan	18.0	1170	34.0	8.1	5.1 ± 6.3	51.2 ± 4.5	−90 ± 17%
634 Morgan	19.7	1170	34.7	7.3	6.0 ± 5.6	54.4 ± 4.8	−89 ± 16%
Carroll	9.12	161	33.7	8.2	280 ± 15	79.4 ± 5.3	+252 ± 27%
Pennsylvanian shales							
Viking A	1.17	51	3.7	13.6	1561 ± 58	27.5 ± 1.9	+5575 ± 439%
Viking B	38.1	402	133	6.1	293 ± 14	274 ± 23	+7.0 ± 10%
Viking D	7.93	77	56.0	11.7	481 ± 24	159 ± 10	+203 ± 21%
Columbia E	29.9	173	61.4	6.8	296 ± 25	148 ± 11	+100 ± 20%
Columbia F	24.4	159	73.7	8.1	308 ± 14	169 ± 12	+82 ± 13%

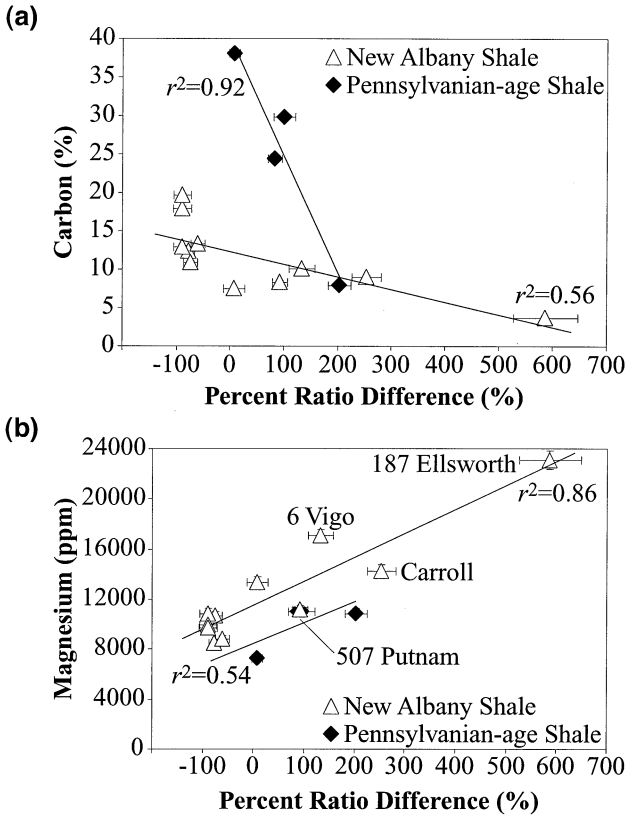

Fig. 3. Percent ^{36}Cl ratio difference as a function of (a) carbon and (b) magnesium. The Viking A sample is not shown on these graphs because of its presumed contamination with bomb-pulse ^{36}Cl. The New Albany Shale samples labeled in (b) are referenced in the text.

heterogeneity in the shales. When an α particle is formed through decay of a radioactive nuclide, that nuclide must have a favorable placement relative to the light elements of the rock

Table 4. Comparison of ^{238}U activities to ^{226}Ra activities.

Sample	U (ppm)	^{238}U activity[a] (pCi/g_{rock})	^{226}Ra activity[b] (pCi/g_{rock})
New Albany Shales			
6 Vigo	12.7	4.24 ± 0.23	4.09 ± 0.37
187 Antrim	28.4	9.48 ± 0.51	9.41 ± 0.82
187 Ellsworth	9.0	3.00 ± 0.16	2.98 ± 0.36
428 Harrison	54.5	18.2 ± 1.0	16.7 ± 1.2
432 Harrison	45.2	15.1 ± 0.8	13.5 ± 1.0
611 Harrison	39.1	13.1 ± 0.7	12.5 ± 0.9
507 Putnam	37.5	12.5 ± 0.7	11.2 ± 0.9
554 Sullivan	23.4	7.81 ± 0.42	8.29 ± 0.74
628 Morgan	34.0	11.3 ± 0.6	12.5 ± 1.2
634 Morgan	34.7	11.6 ± 0.6	11.8 ± 1.0
Carroll	33.7	11.2 ± 0.6	11.1 ± 0.8
Pennsylvanian shales			
Viking A	3.7	1.23 ± 0.07	1.84 ± 0.27
Viking B	133	44.4 ± 2.4	45.6 ± 3.1
Viking D	56.0	18.7 ± 1.0	17.6 ± 1.2
Columbia E	61.4	20.5 ± 1.1	21.3 ± 1.5
Columbia F	73.7	24.6 ± 1.3	23.1 ± 1.5

[a] Calculated from uranium concentration.
[b] Measured using γ spectrometry.

Table 5. Neutron and α travel lengths in the shales.

Sample	Travel length for: Fast neutrons (m)	Thermal neutrons (m)	Total neutron travel length (m)	Travel length for the ^{212}Po 8.784 MeV α[a] (μm)
New Albany Shales				
6 Vigo	2.5	0.30	2.8	15.7
187 Antrim	2.3	0.35	2.7	14.7
187 Ellsworth	2.7	0.32	3.0	14.2
428 Harrison	2.5	0.34	2.8	15.7
432 Harrison	2.5	0.32	2.8	15.1
611 Harrison	2.5	0.32	2.8	15.3
507 Putnam	1.8	0.29	2.1	14.7
554 Sullivan	2.6	0.32	2.9	15.1
628 Morgan	1.9	0.32	2.2	15.4
634 Morgan	1.8	0.33	2.1	15.8
Carroll	2.1	0.34	2.4	15.1
Pennsylvanian shales				
Viking A	2.0	0.34	2.3	13.5
Viking B	1.8	0.47	2.3	18.0
Viking D	1.6	0.33	1.9	14.4
Columbia E	1.8	0.45	2.3	16.8
Columbia F	1.7	0.38	2.1	16.2

[a] This α particle has the highest energy of the alphas in the three naturally occurring decay chains and thus represents the maximum travel distance expected in the (assumed chemically homogeneous) shale.

to produce a neutron through an (α,n) reaction (Andrews et al., 1991). If the rock contains substantial aluminum, for example, but the aluminum is contained in minerals sufficiently removed from α-producing radioactive nuclides, then the calculation will assign too much weight to aluminum with respect to neutron production. Thus, if the rock is chemically heterogeneous on a similar scale as the travel length of the α particle, differences can arise between measured and calculated ^{36}Cl ratios. The calculation algorithm for α particle travel distances is included in the Appendix, as is the calculation algorithm for neutron travel distances; the results of these calculations are presented in Table 5. As can be seen in this table, step 3 in the ^{36}Cl production process is unlikely to be affected by chemical heterogeneity. The long neutron travel length in the shales ensures that neutrons travel across all mineral associations in the rock, effectively seeing a chemically homogeneous sample (Martel et al., 1990). The α range, however, is on the order of microns in these shales. This extremely short range prompted the elemental mapping of one of the shales.

3.3. Elemental Map of the Viking B Shale

To address the scale of chemical heterogeneity, an elemental map was constructed by electron microprobe for the Pennsylvanian Viking B sample. The fragment of shale used for the map is shown in a backscattered image in Figure 1a; the black rectangle outlines the boundary of the elemental map, and Figure 1b shows the backscattered image of the elemental map area. In these images, darker areas represent low atomic weight elements, and lighter areas represent higher atomic weight elements. In general, the dark areas correspond to carbonaceous material, whereas light swaths show clay minerals, and light specks are quartz, pyrite, dolomite, apatite, or calcite. Alumi-

num, silicon, oxygen, magnesium, potassium, and carbon were the elements chosen for mapping because these elements are responsible for 80 to 90% of the calculated (α,n) process neutron production due to uranium. The elemental maps of carbon, aluminum, magnesium, and silicon are included in Figure 2. Oxygen maps almost identically to silicon and is not included, while potassium follows aluminum very closely and is also not included here. These maps show that carbon dominates and that silicon and aluminum overlap but are confined to areas of low or no carbon. With oxygen and potassium following silicon and aluminum, it is evident that these elements indicate the presence of clay minerals. Magnesium shows significant correlation to the swaths of clay material but also has an important presence in dolomite, as seen by the number of bright circular blebs on the magnesium map. The carbonaceous material and the clay minerals occupy physically exclusive areas of the shale. And as can be seen from the scale of the elemental maps, the carbonaceous material and the clay minerals are chemically heterogeneous on a scale of tens of microns.

4. DISCUSSION

4.1. Macroheterogeneity in the Shales

A comparison between the measured and calculated ^{36}Cl ratios in Table 3 calls into question the accuracy of the calculation algorithm, at least for these carbonaceous shales. As can be seen from Figure 2 and Table 5, the scale of the chemical heterogeneity in these shales is similar to the range of α particles. This situation implies that it is the production of neutrons through the (α,n) process that could be causing either excess neutron production or suppressed neutron production, depending on the physical-chemical makeup of the shale. Figure 2 shows the distinct separation between organic matter and clay minerals in the shales. Carbon is a logical element, representing organic material, to compare to the percent ratio difference. As a representative of clay minerals, aluminum or silicon would appear to be the logical choices. However, the relationship between the percent ratio difference and aluminum, silicon, and potassium is flat and therefore uninstructive. Magnesium shows the best correlation to the percent ratio difference for the New Albany Shale samples, and its inclusion in both clay minerals and dolomite blebs provides more latitude in interpreting ^{36}Cl production in these shales. The relationships between the percent ratio difference and the carbon and magnesium contents in the shales are shown in Figure 3.

As discussed in the "Introduction," carboxylic acid functional groups in organic matter can complex with uranium, concentrating it in the organic fraction in carbonaceous shales. Thus, splitting the shales into a uranium-bearing organic fraction and a clay mineral fraction is a reasonable division to explain the differences between measured and calculated ^{36}Cl ratios. The clay minerals contain high-neutron-yield elements such as aluminum and magnesium, as well as prodigious quantities of lower yield elements such as silicon and oxygen. (See Table 6 for neutron yields.) The carbonaceous material of these shales contains carbon with associated oxygen—although the bulk of the oxygen mapped with silicon—and hydrogen as well as organophile elements such as phosphorous, chlorine, and pyritic iron and sulfur. In general, the carbonaceous material is composed of low-neutron-yield elements, and the clay minerals are composed of high-neutron-yield elements. Chemical heterogeneity is present in these shales on the same scale as the α particle travel distance, as shown in Figure 2. Consequently, the placement of the α emitter, whether in organic or in clay, can limit the suite of elements that an α particle can traverse. As the carbon content rises, a large fraction of α particles originating in the organic matrix are constrained to interact with low-neutron-yield elements in that matrix. These α particles are isolated from the high-neutron-yield elements contained within the clay minerals, in direct opposition to the chemical homogeneity assumption of the calculation algorithm. Conversely, as the carbon content falls, uranium is still concentrated in the organic matter, but with less of the organics to traverse, α particles have a much greater probability of interacting with high-neutron-yield elements contained within the clay minerals. This explanation is qualitative but can be tested through some simple modifications to the calculation algorithm.

Table 6. Neutron yields[a] and elemental associations.

Z	Element	Neutron yield per ppm uranium (neutrons g^{-1} yr^{-1})	Neutron yield per ppm thorium (neutrons g^{-1} yr^{-1})	Primary elemental association
3	Lithium	23.8	10.4	Clay
4	Beryllium	265	91.2	Clay
5	Boron	62.4	19.7	Clay
6	Carbon	0.453	0.177	Organic
8	Oxygen	0.235	0.0831	Clay
9	Fluorine	41.2	16.2	Organic
11	Sodium	12.5	5.89	Clay
12	Magnesium	5.81	2.54	Clay
13	Aluminum	5.09	2.55	Clay
14	Silicon	0.684	0.335	Clay
15	Phosphorous	0.860	0.572	Organic
16	Sulfur	0.174	0.103	Organic
17	Chlorine	1.31	0.793	Organic
19	Potassium	0.116	0.0798	Clay
20	Calcium	0.0379	0.0262	Organic
26	Iron	0.184	0.203	Organic

[a] Calculated by multiplying the α production per year per parts per million uranium or thorium by the neutron yield per α particle. Neutron yields per α were taken from Heaton et al. (1989) except for P, S, Cl, K, and Ca. For these five elements, R. Heaton (private communication) used the thick target yields for the (α,n) reaction from Woosley et al. (1975); the cross sections of a Hausser-Feshbach calculation were integrated over energy with the stopping power parameterization of Ziegler et al. (1985) using a simple Runga-Kutta integration.

4.2. Important Aspects of the Calculation Algorithm and the Creation of the Organic-Clay Heterogeneous Model

The complete algorithm for the calculation of the ^{36}Cl ratio is presented in the Appendix. The algorithm works on the assumptions that the radioactive decay chains are in secular equilibrium and that the rock is chemically homogeneous. Although the first assumption has been confirmed for these shales, the second has been shown pictorially to be untrue. With the scale of chemical heterogeneity on the same scale as the α particle travel length, it would appear that neutron pro-

duction through the (α,n) process can be modeled in the shales by splitting the rock into organic and clay mineral fractions and calculating neutron production separately for each fraction.

Neutron production for the entire rock can be calculated using

$$P_n = {}^{238}N\lambda_{sf}\nu + a[U] + b[Th], \quad (5)$$

where ^{238}N is the number of ^{238}U atoms per gram of rock, λ_{sf} is the spontaneous fission decay constant for ^{238}U (8.5×10^{-17} yr^{-1}), ν is the average number of neutrons (2.2) emitted per spontaneous fission of ^{238}U, and [U] and [Th] are the uranium and thorium concentrations (in ppm) for the rock matrix (Andrews et al., 1989). The first term of this equation represents neutron production by spontaneous fission and is thus the minimum neutron producing capability of the rock. The coefficients *a* and *b* in Eqn. 5 are the neutron yields related to the light element composition of the matrix (in neutrons per gram of rock per year per ppm U or Th) and are calculated from the following relationships:

$$a = \frac{\sum_i S_i F_i Y_i^U}{\sum_i S_i F_i} \quad (6)$$

and

$$b = \frac{\sum_i S_i F_i Y_i^{Th}}{\sum_i S_i F_i}, \quad (7)$$

where S_i is the mass stopping power of element *i* (in MeV cm^2 g$_i^{-1}$) for an α particle of some chosen energy (MeV), F_i is the fractional abundance for element *i*, and Y_i^U and Y_i^{Th} are the neutron yields for element *i* per part per million of U and Th in equilibrium with their daughter products (Andrews et al., 1986), as included in Table 6. In a bulk-rock-based calculation, the fractional abundance (F_i) would be the same for each element in the calculation of both *a* and *b*. For these carbonaceous shales, however, the organic and clay mineral fractions are very distinct in chemical makeup and can be separated, associating the elements that make up the organic fraction with elemental neutron yields for uranium and the elements that make up the clay mineral fraction with elemental neutron yields for thorium. (Thorium concentration as a function of aluminum registered an r^2 of 0.51 for the 11 samples of the New Albany Shale and 0.99 for the 5 samples of the Pennsylvanian shale.)

The associations for each element listed in Table 6, whether organic or clay, were used as a basis for separate neutron production calculations for the organic and clay mineral fractions. (For the homogeneous calculation, oxygen was calculated as the difference between 1 million ppm and the bulk-rock concentrations of the elements listed in Table 6. This value of oxygen was subsequently used in the calculation of the end-member organic and clay mineral fractions.) The bulk-rock concentrations of carbon, fluorine, phosphorous, sulfur, chlorine, calcium, iron, and 20% of the oxygen were redistributed to 1 million ppm, creating the organic fraction that was used in the calculation of the *a* coefficient. The bulk-rock concentrations of lithium, beryllium, boron, sodium, magnesium, aluminum, silicon, potassium, and 80% of the oxygen were redistributed to 1 million ppm, creating the clay mineral fraction that was used in the calculation of the *b* coefficient. The oxygen content mapped very similar to silicon in Figure 2 and thus is controlled by the clay minerals. The organic fraction, however, does contain oxygen, hence the percentage split described above. Because the organic and clay mineral fractions are not isolated onto themselves with respect to the ultimate target of α particles originating in each fraction, a volume-based weighting factor was used to include in the uranium-organic calculation a fraction of the elements assigned to clays and to include in the thorium-clay calculation a fraction of the elements assigned to organics. A density of 1.3 g/cm^3 was applied to the organic carbon content, and a density of 2.7 g/cm^3 was applied to the summation of the aluminum, silicon, oxygen, potassium, sodium, and magnesium concentrations. The percentage volumes of the organics and the clay minerals were then calculated from the total volume. Other elements, such as iron, sulfur, and oxygen, could have been added to carbon in the calculation of the volume occupied by organics. However, the calculation is not very sensitive to these weighting factors, and as such, a shift in volume of 5 to 10% has very little effect on the final ratio. The results of this calculation are presented in Table 7, under the heading "Heterogeneous calculated ^{36}Cl/Cl: organic-clay mineral division only." Also included in this table are the organic and clay mineral weighting factors calculated from the volumes of the organic and clay mineral fractions. For the 6 Vigo shale, the organics occupy 19% of the volume, and the clays occupy 81% of the volume. From a weighting perspective, it was assumed that α particles originating in the organic fraction would exclusively interact with 19% of the end-member organic assemblage and with 81% of the end-member clay assemblage with respect to (α,n) neutron production. The fractional abundances for the *a* coefficient were weighted accordingly. Similarly, it was assumed that the α particles originating in the clay fraction would exclusively interact with 81% of the end-member clay assemblage and with 19% of the end-member organic assemblage with respect to (α,n) neutron production, and the fractional abundances for the *b* coefficient were also weighted accordingly. These weighting factors were also used to adjust the uranium and thorium concentrations to their respective fractions. For the 6 Vigo sample, the 12.7 bulk-rock ppm uranium was redistributed to an organic basis using the 19% of the rock that was organic. Similarly, the 7.9 bulk-rock ppm thorium was redistributed to a clay mineral basis using the 81% of the rock that was clay. Because neutron production in the separate fractions had to be put back on a whole-rock basis using the same weighting factors, concentrating the radioactive elements in their respective fractions was insensitive to the weighting factor.

As can be seen from the comparison of the homogeneous calculated ratios to the calculated ratios assuming an organic-clay division, the majority of the shales do not show significant changes to their calculated ^{36}Cl ratios. Absolute differences of 1 to 2×10^{-15} are typical for the New Albany Shale samples, whereas the Pennsylvanian shales show a greater range of 1 to 8×10^{-15}. The general assumption stated above, that as the carbon content rises, α particles originating in the organic fraction from uranium will be isolated from the high-yield

Table 7. Model parameters and results.

Sample	Adjusted measured ^{36}Cl/Cl ($\times 10^{-15}$)	Homogeneous calculated ^{36}Cl/Cl ($\times 10^{-15}$)	Heterogeneous calculated ^{36}Cl/Cl: Organic-clay mineral division only ($\times 10^{-15}$)	Heterogeneous calculated ^{36}Cl/Cl: Organic-clay mineral-francolite ($\times 10^{-15}$)	Heterogeneous calculated ^{36}Cl/Cl: Francolite only ($\times 10^{-15}$)	Bulk-rock U (ppm)	Total U in franco-lite (%)	Bulk-rock Cl (ppm)	Total Cl in francolite (%)	Organic weighting factor (%)	Clay weighting factor (%)
New Albany Shales											
6 Vigo	61.1 ± 5.5	26.2	27.8	61.5	0.8	12.7	90	325	5	19	81
187 Antrim	56.1 ± 9.6	52.1	54.1	56.1	0.4	28.4	5	597	5	15	85
187 Ellsworth	154 ± 9	22.5	23.9	49.2	0.2	9.0	100	337	5	6.7	93.3
428 Harrison	21.0 ± 4.7	93.3	95.6	27.7	14.6	54.5	5	741	87	26	74
432 Harrison	18.9 ± 6.2	75.7	77.2	20.3	22.7	45.2	5	819	90	22	78
611 Harrison	25.3 ± 5.7	63.6	64.4	25.8	20.1	39.1	5	748	75	26	74
507 Putnam	134 ± 7	69.8	72.0	136	1.2	37.5	60	266	5	17	83
554 Sullivan	4.3 ± 4.8	41.5	41.9	7.4	12.3	23.4	5	776	100	25	75
628 Morgan	5.1 ± 6.3	51.2	51.2	5.7	17.1	34.0	5	1170	100	33	67
634 Morgan	6.0 ± 5.6	54.4	54.1	13.8	13.5	34.7	5	1170	83	36	64
Carroll	280 ± 15	79.4	81.8	206	1.6	33.7	100	161	5	19	81
Pennsylvanian shales											
Viking A	1561 ± 58	27.5	29.4	48.7	0.3	3.7	100	51	5	2.4	97.6
Viking B	293 ± 14	274	266	283	4.4	133	5	402	5	60	40
Viking D	481 ± 24	159	164	387	4.6	56.0	100	77	5	16	84
Columbia E	296 ± 25	148	145	299	5.2	61.4	80	173	5	50	50
Columbia F	308 ± 14	169	168	307	5.4	73.7	80	159	5	43	57

elements in the clay fraction, and vice versa, is borne out, though weakly. The two Morgan County samples, which have the highest carbon contents of the New Albany Shale samples, show either no change or a slight drop in ratio; all the other lower carbon New Albany Shale samples show a rise in the ratio. For the Pennsylvanian shales, the high-carbon Viking B and Columbia E and F samples show decreases in ratio, whereas the low-carbon Viking A and D samples show a rise in ratio. When compared to the measured ^{36}Cl ratios, the heterogeneous ratio calculated using an organic-clay split approaches the measured ratio only for the 187 Antrim sample, whose homogeneous calculated ratio was already comparable (within error) to the measured ratio. For all other samples the simple division of the shale into an organic fraction and a clay mineral fraction does not explain the measured ratios for these shales. The redistribution of the bulk-rock elements using the weighting factors in Table 7 was not significant enough to either concentrate high-neutron-yield elements in the α flux or isolate high-neutron-yield elements from the α flux. In addition, this division does not address the fact that samples such as 554 Sullivan, 628 Morgan, and 634 Morgan have ^{36}Cl ratios lower than the minimum ratio set by the presence of spontaneous fission neutrons from ^{238}U. The organic-clay split only addresses neutron production from the (α,n) process, and to explain very low ^{36}Cl ratios, another physical heterogeneity must be present.

4.3. The Accessory Mineral Apatite/Francolite as a Control on ^{36}Cl Production

Two interesting chemical relationships are presented in Figure 4. Figure 4a shows the dependence of the chlorine content on the phosphorous content for the shales. Also included in this figure are the regions of positive and negative percent ^{36}Cl ratio difference for the New Albany Shale samples. Figure 4b shows the dependence of the chlorine content on the carbon content for the shales, also including the regions of positive and negative percent ^{36}Cl ratio difference for the New Albany Shale samples. As can be seen from both plates of this figure, as the carbon and phosphorous contents rise, the chlorine content also rises. Looking at the percent ^{36}Cl ratio differences, shales that have low phosphorous and carbon have positive percentage ratio differences, indicating that the measured ^{36}Cl ratio was greater than the calculated ^{36}Cl ratio for these samples. For the shales that have higher phosphorous and carbon contents, the percent ratio differences are negative, indicating that the measured ^{36}Cl ratio was less than the calculated ^{36}Cl ratio for these samples. An organic-clay heterogeneous split does not explain measured ^{36}Cl ratios that are different from homogeneous calculated ratios, as demonstrated above. Thus, organic carbon does not control the ^{36}Cl ratio, as implied in Figure 4b; it is phosphorous that is controlling the ^{36}Cl ratio. The phosphorous in these shales is included in accessory phosphate minerals such as apatite, $Ca_5(PO_4)_3(F,Cl,OH)$, or francolite, represented by $Ca_{10}[(PO_4)_{6-x}(CO_3,F)_x](F,Cl,OH)_2$ (Chang et al., 1998). Another possible source of phosphorous is monazite, (Ce, La,Nd,Th)PO_4, found as a late-stage diagenesis replacement of carbonate fluorapatite (francolite) in Ordovician black shales of the southern Welsh (UK) basin by Lev et al. (1998). What should be noted about apatite and francolite is that they include chlorine (after fluorine in importance) as a structural element. And all these minerals can concentrate REEs (see analyses in Lev et al., 1998, Table 1; Lev et al., 1999, Table 1; Chang et al., 1998, Tables 39–44) and uranium, though francolite and monazite are more effective in their concentration of uranium than apatite (for francolite, see analysis in Fisher and Wignall, 2001, Table 1; for monazite, see analyses in Lev at al., 2000, Table 3;

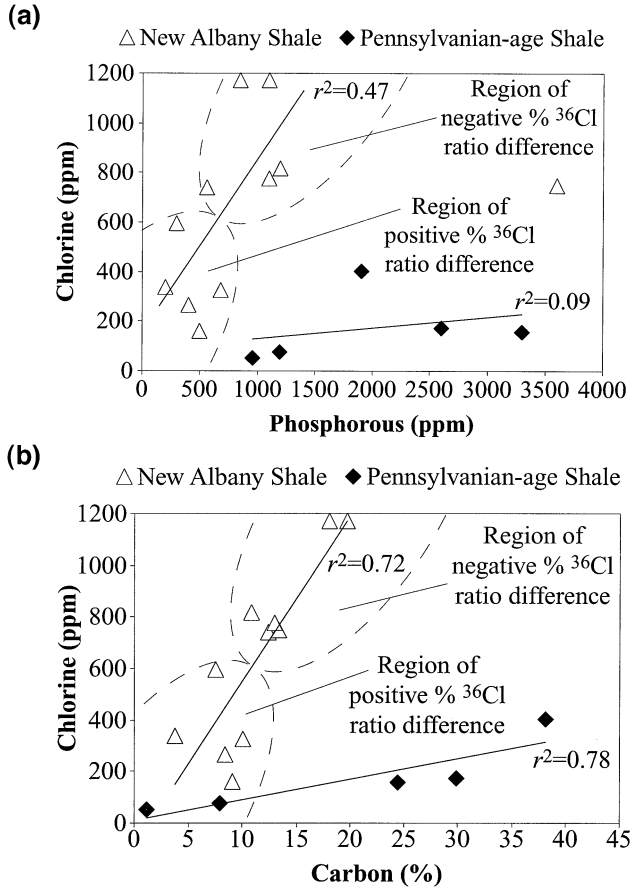

Fig. 4. Chlorine as a function of (a) phosphorous and (b) carbon. The coefficient of determination for the New Albany Shale samples in (a) does not include the outlying sample. Dashed boundaries enclose areas of positive or negative percent ^{36}Cl ratio difference for the New Albany Shale samples and indicate their trends with respect to chlorine relative to carbon and phosphorous. The outlying New Albany Shale sample in (a) has a negative percent ratio difference. All of the Pennsylvanian shales have positive percent ratio differences.

Chang et al., 1998, Tables 43–44). Thus, as a result of its ability to concentrate uranium and REEs and to incorporate fluorine and chlorine, francolite was chosen as a third source of neutron production, in addition to neutron production from the organic-clay split, in the heterogeneous ^{36}Cl calculation algorithm.

Two processes are at work in francolite with respect to ^{36}Cl production. One, the concentration of uranium in close proximity to high-neutron-yield fluorine (see Table 6), can create a neutron production source in the mineral. Two, the concentration of REEs such as samarium, europium, gadolinium, and dysprosium—all having very high thermal neutron absorption cross sections—in proximity to chlorine has the net effect of shielding the chlorine from thermal neutrons, leading to the suppression of ^{36}Cl production. For the purposes of the calculation, all bulk-rock phosphorous in the shales was used to create francolite—having a formula of $Ca_5(PO_4)_2CO_3F_2$—and the other major elements were added stoichiometrically on the basis of this formula. It should be noted that this formula, involving the substitution of a full phosphate radical with a carbonate plus fluorine, represents an idealized francolite. Although Chang et al. (1998, Table 42) did present an analysis that includes $F_{1.47}$, most francolite analyses do not contain this much fluorine. The stability of fluorapatite/francolite over chlorapatite/francolite means that the model francolite must start out as a fluorfrancolite. The exceptions were the 611 Harrison, Viking B, Columbia E, and Columbia F samples, in which there was insufficient fluorine to complete the mineral and it was necessary to fill the balance using hydroxyl. The bulk-rock concentrations of the REEs samarium, europium, gadolinium, and dysprosium were also added to the mineral. The concentrations of uranium and chlorine could be varied in the francolite, and the concentrations of all elements were redistributed to 1 million ppm for each change in uranium and chlorine. The organic fraction was assumed to host the bulk-rock uranium, and uranium added to francolite was subtracted from the uranium available for neutron production in the organic fraction. For the calculation of the *a* coefficient of (α,n) neutron production for francolite, carbon, fluorine, phosphorous, chlorine, and calcium were used, while the REE and uranium concentrations were dropped and oxygen picked up the balance. To return the neutron production due to francolite back to a whole-rock basis, the bulk-rock concentrations of the elements assigned to francolite were added together to determine the micrograms of francolite per gram of rock, which was applied to francolite's neutron production. The chlorine concentration was designed to be variable in the francolite, and the addition of chlorine had two effects on the calculation. The first effect was the alteration in (α,n) neutron production through the replacement of fluorine by chlorine in the calculation of the *a* coefficient. This replacement had the result of lowering the neutron production because of the much lower neutron yield of chlorine vs. fluorine (Table 6). Second, the assumption was made that all chlorine added to francolite was effectively removed from the ^{36}Cl production process because of shielding by the REEs. (The validity of this assumption will be discussed below.) In the final equation of the ^{36}Cl production process (see the Appendix for equation development and full explanation of symbols),

$$R_{eq} = \Phi_{n(th)} \frac{1}{\lambda_{36} N_{Cl}} (\sigma_{35} N_{35} + \sigma_{39} N_{39}) + \Phi_{n(epi)} \frac{1}{\lambda_{36} N_{Cl}} (I_{35} N_{35} + I_{39} N_{39}), \quad (8)$$

N_{35} represents the number of atoms of ^{35}Cl available (on an atom-per-gram basis) for thermal (th) and epithermal (epi) neutron absorption to form ^{36}Cl, while N_{Cl} represents the total number of chlorine atoms in the rock (on an atom-per-gram basis). Thus, any chlorine added to francolite lowers N_{35} in the numerator of Eqn. 8 while maintaining the full bulk-rock N_{Cl} in the denominator, effectively lowering the calculated ^{36}Cl ratio.

The results of this calculation are presented in Table 7, under the heading "Heterogeneous calculated ^{36}Cl/Cl: organic-clay mineral-francolite." Also included in this table are the bulk-rock uranium and chlorine contents, as well as what percentages of the bulk rock uranium and chlorine were assigned to francolite to achieve the listed ratios. For both uranium and chlorine, the starting point in the construction of francolite was to put 5% of the bulk-rock concentrations of these elements

into the mineral and adjust upward. Adding uranium to francolite increases neutron production for the whole rock through the (α,n) reaction of α particles with high-neutron-yield fluorine. Adding chlorine to francolite decreases the production of ^{36}Cl by isolating ^{35}Cl in the midst of REEs having high thermal neutron cross sections. Chlorine was varied (in increments of 5%) in francolite for shales that had measured ^{36}Cl ratios less than the homogeneous calculated ratios and needed to lower ^{36}Cl production. For the 428 Harrison and the 634 Morgan shales, all fluorine was replaced by chlorine, creating an end-member chlorfrancolite. Uranium was varied (in increments of 5%) in francolite for shales that had measured ^{36}Cl ratios greater than the homogeneous calculated ratios and needed to raise ^{36}Cl production.

The results of this calculation are much more in line with the measured ^{36}Cl ratios, as can be seen from Table 7. It should be noted that these calculations are a means of providing a framework of explanation for the measured ^{36}Cl ratios, using as an initial starting point the homogeneous calculated ratios and shale chemistry. By performing the calculations within the mineralogical constraints of the shales and achieving a result conforming to the independent measurements, the importance of an accessory mineral such as francolite as a necessary part of the production process is confirmed. Having to place 100% or close to 100% of uranium or chlorine into francolite, however, is not completely satisfactory, because the complete concentration of these elements into an accessory mineral implies that the heterogeneous calculation model could be overlooking other processes, processes responsible for either neutron production or chlorine isolation. Four of the New Albany Shale samples provide a hint at a possible neutron production process outside of the heterogeneous model. These are the 6 Vigo, 187 Ellsworth, 507 Putnam, and Carroll samples, all labeled in Fig. 3b, showing the relationship between the percent ^{36}Cl ratio difference and magnesium. All these samples have very positive percent ratio differences, indicating actual ^{36}Cl production higher than that expected from the homogeneous calculation. On a homogeneous basis, and for the shales as a whole, neutron production from aluminum, carbon, silicon, potassium, and oxygen accounts for 80% of the calculated total, and neutron production due to magnesium is typically in the range of 10% of the calculated total. The elemental maps in Figure 2 show that these elements are distinctly separated into clay mineral and organic fractions. The exception is magnesium, which shows significant concentration in dolomite. Looking at the trend of the percent ^{36}Cl ratio difference vs. magnesium, as the magnesium content increases, the measured ^{36}Cl ratio also increases but at a rate not explained by the homogeneous calculated ^{36}Cl ratio. Dolomite is not a bearer of uranium. But concentrating magnesium (with a neutron yield of 5.81 neutrons per gram of Mg per ppm U per year) in dolomite and placing the dolomite in either the uranium-bearing organic fraction or in contact with uranium-bearing phosphate minerals could produce a neutron production source similar to francolite. Determining the efficacy of neutron production of dolomite vs. francolite is a difficult proposition; francolite has an internal α particle source, but dolomite would have to rely on an external α particle source. Determining the whole-rock neutron production attributable to dolomite as compared to francolite is also qualitative. The heterogeneous model calculated neutron production due to francolite and then scaled that production down to a whole-rock basis. The 6 Vigo sample, for instance, contained a calculated 5400 μg francolite per gram of total rock. With a total magnesium content of 17,100 ppm, and assuming that half of that magnesium was in dolomite, then 6 Vigo contains close to 65,000 μg dolomite per gram of total shale, a much larger neutron production base than francolite. However, as mentioned above, this dolomite needs an external α source, and it is unclear whether the enrichment of uranium into the organic fraction would be significant enough, or whether some other enrichment process would be needed, such as precipitated uraninite or authigenic phosphate minerals in proximity to dolomite blebs, to produce the α flux needed for a noticeable increase in neutron production. The results of Fig. 3b, however, do indicate that magnesium is experiencing the increased α flux and that increased ^{36}Cl production is occurring.

One the opposite side are the shales with a lower ^{36}Cl ratio than the homogeneous calculated ratio. Quite a few of the New Albany Shale samples needed a large percentage of chlorine added to francolite to shield them from the thermal neutron flux, according to the heterogeneous model. This, as mentioned above, is not completely satisfactory. However, chlorine in organic association has no protection from thermal neutrons. The REEs, which can shield chlorine from the thermal neutron flux, are in phosphate minerals. For all the shale samples, concentrating the bulk-rock REEs into francolite provides a higher thermal neutron absorbance cross section than that of ^{35}Cl, even for the complete concentration of chlorine into francolite. Thus, the REEs do shield ^{35}Cl from the thermal neutron flux, and the assumption that chlorine added to francolite is effectively removed from the ^{36}Cl production process is valid. What the REEs do not do, however, is shield chlorine from resonance capture in the epithermal neutron flux. The third column under the heading "Heterogeneous calculated ^{36}Cl/Cl, i.e., francolite only" shows the calculated ratio within francolite, based on the total neutron production for the rock as calculated in the organic-clay mineral-francolite model. The ratio as shown has been redistributed to a whole-rock basis and is comparable to the other heterogeneous ratios. For most of the shales, the addition of the francolite ratio component is minimal. For the shales in which a significant quantity of chlorine was added to francolite, the ratio is similar to that of the organic-clay mineral-francolite model, and the addition of these two ratios puts the heterogeneous calculated ^{36}Cl ratio unacceptably higher than the measured ratio. The overwhelming majority of the ^{36}Cl ratio shown in Table 7 under the "Francolite only" column is due to the epithermal neutron flux, not the thermal neutron flux. Most of the New Albany Shale samples had 90 to 95% of their francolite-only ratio formed by resonance capture, with the 611 Harrison sample being lowest with 80% of the ratio formed by resonance capture. For the Pennsylvanian shales, typically 80% of the francolite-only ratio was formed by resonance capture. There are two implications of high ^{36}Cl ratios attributable to production in francolite. First, this model finding implies that the measured ^{36}Cl ratios (included in Tables 2, 3, and 7) could represent ratios dominated by the chlorine in organic association—chlorine that was oxidized from the organic matrix and collected for ^{36}Cl measurement. The experimental method, oxidation of organic matter using hydrogen peroxide to release the assumed organically

bound chlorine on the basis of the relationship in Figure 4b, was not necessarily suitable for the quantitative dissolution of phosphate minerals (for which a mild nitric acid solution would have been more preferable) to release the chlorine they might include. However, the fact that a relationship does exist between chlorine, phosphorous, and the percent ratio difference shown in Figure 4a does imply that substantial chlorine was released from phosphate minerals during the oxidation of the shale. The second implication is discussed below, namely, that unmeasured organic hydrogen may provide rapid thermalization of neutrons, providing a much lower epithermal neutron flux than calculated.

4.4. Heterogeneity and the Production of ^{36}Cl

What the previous discussion about the heterogeneous calculation model makes clear is that chemical and physical heterogeneity in these shales controls the production of ^{36}Cl. The heterogeneous model, though dictated by a combination of chemical relationships (such as in Fig. 4) and physical relationships (such as in Figs. 1 and 2), is too simple to provide a complete explanation for the measured ^{36}Cl ratios. This point is emphasized by the necessity of assigning very large percentages of uranium or chlorine into francolite to explain the measured ^{36}Cl ratios. Magnesium appears to provide a controlling influence in the production of ^{36}Cl, especially for samples such as 187 Ellsworth and Carroll, for which the heterogeneous model cannot generate enough neutron production to bring the calculated ratio up to the measured ratio. But magnesium is not represented in the model. In fact, there are a host of mineralogical variables that cannot be modeled because of insufficient information provided by a bulk-rock chemical analysis. Lev et al. (1998) showed that in the black shales of the Welsh Basin (UK), late diagenetic monazite replaced apatite. The replacement was not complete, but the presence of monazite, with respect to the heterogeneous model, is not advantageous. Although monazite can concentrate uranium, thorium, and REEs, it does not contain halogens. In this situation, the heterogeneous model becomes useless, because monazite is both a poor producer of neutrons from the (α,n) process and a nonexistent shield for chlorine, because it does not contain chlorine. However, because monazite only partially replaced apatite in the shales studied by Lev at al. (1998), the monazite (in intimate association with apatite) would effectively form an α production source, perhaps concentrating the shale's thorium in addition to uranium; α particles impinging on apatite would produce a much higher neutron flux than monazite alone. If this is the case, then the heterogeneous model (using francolite) could be producing the correct results but with the wrong phosphate mineral.

In general, the concentration of fluorine is reasonably flat over the range of phosphorous (Table 1), while Figure 4a shows that as the phosphate content rises, the chlorine content also rises. Thus, as the phosphorous content rises and the shales host more francolite, the lower fluorine content relative to phosphorous would indicate that more chlorine is being included in francolite, at the expense of fluorine. The francolite created in the model generally followed this observation, with shales that had high phosphorous and chlorine contents having more chlorine in francolite. Unlike the halogens, which are necessary elements in francolite and can be expected to follow a logical substitution trend with increasing concentration, uranium incorporation in francolite was less logical. The concentration trend of uranium was opposite that of chlorine; for low phosphorous contents, more uranium would need to be incorporated into francolite, and for high phosphorous contents, less uranium would need to be incorporated into francolite. In reality, a very large percentage of the total-rock uranium could be incorporated into francolite without changing the model results. This is because the replacement of fluorine by chlorine reduces neutron production because of chlorine's neutron yield being a factor of 30 less than that of fluorine. Thus, for high-chlorine francolite, a large fraction of uranium could have been incorporated into the mineral, leading to a drop in both neutron production and the ^{36}Cl ratio. The starting point for the heterogeneous model did not have to be 5% uranium assigned to francolite; it could have been 50%, and the differences between the New Albany Shale samples and the Pennsylvanian shales with respect to uranium content in the model francolite would not be so pronounced. Interestingly, the other main substitution possible for fluorine in francolite, hydroxyl, leads to even less neutron production because the neutron yield of oxygen is 175 times less than that of fluorine. This substitution was built into the heterogeneous model but was not used because the variation of chlorine and uranium was more than sufficient to alter the ^{36}Cl ratio. Thus, for low-phosphorous shales that require excess neutron production, the high uranium content of fluorfrancolite would yield that production. For high-phosphorous shales that need less neutron production, the high uranium content in association with the chlorine in francolite would lower the neutron production below fluorfrancolite, but the presence of REEs in the francolite would exert a controlling influence on the ^{36}Cl ratio through shielding of ^{35}Cl. The implication is that although uranium is obviously key in the production of both spontaneous fission neutrons as well as (α,n) process neutrons, the different possibilities for its mineralogical association in trace minerals—apatite, francolite, and monazite in association with apatite—are all favorable for neutron production. But chlorine, through its mineralogical associations, exerts more control on ^{36}Cl production than uranium. The mineralogical association of chlorine with phosphates, and the resulting shielding due to the presence of REEs, can lower the ^{36}Cl ratio even below the minimum expected for the rock due to the presence of spontaneous fission neutrons from ^{238}U.

One aspect of heterogeneity that cannot be ascertained in these shales, with respect to ^{36}Cl production, is the exact organic composition of the organic fraction. The shales were chemically analyzed to obtain a bulk-rock composition, a composition that could be used to perform a homogeneous calculation of the ^{36}Cl ratio. The organic fraction in these shales was not isolated and subjected to a traditional organic analysis to determine C, N, O, H, and S. No published thick-target neutron yields are available for nitrogen, but considering the yields of its neighbors carbon and oxygen in the periodic table, it is expected that the yield of nitrogen would be in the range of 0.2 to 0.4 neutrons per gram of nitrogen per part per million of U per year (see Table 6). As such, a reasonable estimate of 2 to 3% nitrogen in the organic fraction (see Durand and Espitalié, 1976, Table 3; Harwood, 1977, Table 1) would have little impact on the neutron production for the organic fraction

through the (α,n) process. Oxygen, with its low neutron yield but high concentration in these shales, effectively suppresses neutron production in the (α,n) process. A better knowledge of the oxygen composition of the organic fraction would provide a much better grasp on (α,n) process neutron production in the organics. Knowledge of the hydrogen content in the organic fraction is even more important. Hydrogen as an element has not been discussed up to now because it does not produce neutrons in the (α,n) process and because the thermalization of neutrons has not been put forth as a probable cause in the anomalous production of ^{36}Cl. Most of the shales averaged 5000 to 7000 ppm total hydrogen, as calculated from H_2O^+ and H_2O^-; this quantity of hydrogen was typically responsible for 85% of the average scattering cross section used in the calculation of the resonance escape probability. In an analysis of the U.S. Geological Survey reference sample SDO-1, from the Late Devonian Huron Member of the Ohio Shale (Leininger, 1981), H_2O^+ was 4.5% and H_2O^- was 0.69%, roughly comparable in structural water though with lower included water as compared to the New Albany Shale samples (Table 1); organic hydrogen, however, was 13,500 ppm. In organic analyses of Late Devonian Chattanooga shale, McGowan et al. (1983) found that hydrogen directly correlated with organic carbon, whereas for this study, total hydrogen did not correlate with carbon for the New Albany Shale samples and negatively correlated with carbon for the Pennsylvania samples. Thus, it appears that the structural plus included water determined for the shales in this study was most likely to be in association with the clay (inorganic) fraction. The addition of organic hydrogen to inorganic hydrogen in these shales would have an important impact, with respect to the calculation of the scattering cross section. By increasing the scattering cross section (as weighted by the logarithmic energy loss) by a factor of 3, the resonance escape probability increases and the epithermal neutron flux decreases. This has the result of decreasing the contribution to the ^{36}Cl ratio both from resonance absorption due to ^{35}Cl as well as from the ^{39}K(n,α)^{36}Cl reaction because the resonance absorption cross section for the latter reaction is 2 orders of magnitude larger than its thermal absorption cross section. The New Albany Shale samples that have the most negative percent ratio differences are also the highest carbon shales. It also turns out that these shales are the most likely to have high oil and gas yields. The Harrison County samples come from a locality that had numerous producing gas wells during the 19th and 20th centuries (Bassett and Hasenmueller, 1981) and would be expected to have significant organic hydrogen. The Morgan County samples have carbon contents $>$ 18%, and on the basis of the positive linear relationship of $\sim$1 gal oil per ton of shale per percentage organic carbon for the New Albany Shale samples—determined on samples from the same borehole as the 554 Sullivan sample (Meinschein, 1981)—the high-carbon Morgan County samples would be expected to have significant organic hydrogen. These high carbon shales are the ones that needed high chlorine contents in phosphate to shield the chlorine from the thermal neutron flux. As noted above, REEs in phosphate will not shield chlorine from the epithermal neutron flux, and the ratios shown for the francolite in Table 7 show that. However, a threefold increase in hydrogen content for these high carbon shales would have the effect of rapidly thermalizing neutrons, lowering the epithermal neutron flux and reducing ^{36}Cl production due to resonance capture. With respect to the heterogeneous model, the lowered epithermal neutron flux lowers the resonance capture of the chloride residing in francolite, leading to lower ^{36}Cl ratios attributable to francolite than currently shown in Table 7. This is especially true for the samples, for which a large percentage of chlorine was added to francolite to take advantage of the shielding properties of the REEs.

5. CONCLUSIONS

If rock chemistry is to be used to calculate the ^{36}Cl ratio, a more comprehensive chemical analysis may need to be performed to accurately characterize the elemental and mineralogical relationships in the rock. The differences between measured ^{36}Cl ratios and ^{36}Cl ratios calculated using bulk-rock chemical analysis of the carbonaceous shales studied for this work show the necessity of a more detailed chemical analysis. One lesson learned from the heterogeneous model is that the bulk redistribution of elements, based on an organic-clay mineral split, does not lead to significant deviations in ^{36}Cl ratio from the ^{36}Cl ratio as traditionally calculated using assumptions of chemical homogeneity. Bulk redistribution here is defined as the reassignment of elements on a tens of percent scale. What is necessary to achieve large differences between heterogeneous and homogeneous calculated ratios is elemental concentration, such as occurs in the formation of accessory minerals. In addition to the elemental maps made of the area shown in Figure 1b, a qualitative microprobe analysis of accessory minerals in this area was performed. The accessory mineral inventory included pyrite, quartz, calcite, dolomite, apatite-francolite, anatase, and the odd nonferrous sulfide. (It should be noted that apatite-francolite was qualitatively determined by the presence of calcium and phosphorous only.) Of these minerals only apatite-francolite has the rather unique assemblage—with respect to the production of ^{36}Cl—of fluorine and chlorine as essential elements and uranium and REEs as minor, though important, elements. From the perspective of increasing neutron production and thus ^{36}Cl production (relative to the calculation assuming chemical homogeneity), the association of uranium and high-neutron-yield fluorine allows for apatite-francolite to act as a neutron production source. From the perspective of decreasing ^{36}Cl production, the replacement of fluorine by chlorine and the association of REEs with this chlorine can help shield the chlorine from the thermal neutron flux, though not from the epithermal neutron flux. The determination of the ^{36}Cl ratio for mineralogically complex rocks must take into account the possibility that certain accessory minerals can concentrate important elements that can lead to enhanced or suppressed production of ^{36}Cl, with respect to a homogeneous calculation.

Sandstones, siltstones, limestones, and mudstones or shales of average composition do not contain sufficient uranium or thorium to cause significant production of ^{36}Cl in the subsurface. Thus, the ^{36}Cl ratio of groundwater that flows through or along these rock types should be affected only by the expected natural decay of the isotope. When the rock type in contact with groundwater contains $>$ 10 ppm uranium, however, subsurface production of ^{36}Cl can become significant relative to infiltrating ^{36}Cl, and accurate knowledge of the ^{36}Cl content of the rock

becomes very important. Thus, when using ^{36}Cl in groundwater studies where there is confirmed presence of rock types—carbonaceous shales, coals, phosphorites, grantites or pegmatites—that can concentrate uranium, either through organic association, phosphate minerals, uraninite, and so on, care should be taken to obtain the most accurate value of the ^{36}Cl ratio of the rock. In addition to direct measurement using AMS, heterogeneous calculations based upon detailed chemical analysis of the rock provide another option to obtain an accurate ^{36}Cl ratio.

Acknowledgments—We would like to thank the reviewers, F. M. Phillips, John Stone, and especially the anonymous reviewer, for their comments, suggestions, and guidance. We would also like to thank Associate Editor S. Krishnaswami for helpful suggestions during the final stages of review of this paper. The first author would like to thank all the members of the PRIME Lab, who provided invaluable help in the isotope measurements of the shale samples. Dr. Robert Landolt provided valuable help and guidance for the measurement of the ^{226}Ra activities in the shales. Dr. Reto Gieré and Carl Hagar provided much needed assistance with the elemental mapping, and this work was greatly improved through their effort and patience.

Associate editor: S. Krishnaswami

REFERENCES

Andrews J. N., Fontes J.-C., Michelot J.-L., and Elmore D. (1986) In-situ neutron flux, ^{36}Cl production and groundwater evolution in crystalline rocks at Stripa, Sweden. *Earth Planet. Sci. Lett.* **77,** 49–58.

Andrews J. N., Davis S. N., Fabryka-Martin J., Fontes J.-C., Lehmann B. E., Loosli H. H., Michelot J.-L., Moser H., Smith B., and Wolf M. (1989) The in situ production of radioisotopes in rock matrices with particular reference to the Stripa granite. *Geochim. Cosmochim. Acta* **53,** 1803–1815.

Andrews J. N., Florkowski T., Lehmann B. E., and Loosli H. H. (1991) Underground production of radionuclides in the Milk River aquifer, Alberta, Canada. *Appl. Geochem.* **6,** 425–434.

Balashov V. V. (1997) *Interaction of Particles and Radiation with Matter* (trans. Gil Pontecorvo). Springer-Verlag, Berlin, Germany.

Bassett J. L. and Hasenmueller N. R. (1981) Gas production. In *Studies of the New Albany Shale (Devonian and Mississippian) and Equivalent Strata in Indiana* (eds. N. R. Hasenmueller and G. S. Woodward), pp. 85–92. Indiana Department of Natural Resources, Geological Survey.

Beckurts K. H. and Wirtz K. (1964) *Neutron Physics*. Springer-Verlag, New York.

Bentley H. W., Phillips F. M., and Davis S. N. (1986) Chlorine-36 in the terrestrial environment. In *Handbook of Environmental Isotope Geochemistry, Vol. 2, The Terrestrial Environment B* (eds. P. Fritz and J. C. Fontes), pp. 427–480. Elsevier, Amsterdam, the Netherlands.

Breger I. A., Hatcher P. G., Romankiw L. A., Miknis F. P., and Maceil G. E. (1983) Upper Devonian black shales of the Eastern United States: Organic geochemical studies—Past and present. In *Geochemistry and Chemistry of Oil Shales, ACS Symposium Series 230* (eds. F. P. Miknis and J. F. McKay), pp. 181–198. The American Chemical Society, Washington DC.

Bustin R. M., Mastalerz M., and Wilks K. R. (1993) Direct determination of carbon, oxygen and nitrogen content in coal using the electron microprobe. *Fuel* **72,** 181–185.

Chang L. L. Y., Howie R. A., and Zussman J. (1998) *Rock-Forming Minerals, Vol. 5B: Non-Silicates: Sulphates, Carbonates, Phosphates, Halides*. The Geological Society, London.

Chmiel G. (1999) *Subsurface Production of Chlorine-36 in Carbonaceous Shales*. M.S. thesis, Purdue University.

Durand B. and Espitalié J. (1976) Geochemical studies on the organic matter from the Douala Basin (Cameroon)—II. Evolution of kerogen. *Geochim. Cosmochim. Acta* **40,** 801–808.

Fabryka-Martin J. T. (1988) *Production of Radionuclides in the Earth and Their Hydrogeologic Significance, With Emphasis on Chlorine-36 and Iodine-129*. Ph.D. dissertation, University Arizona.

Fabryka-Martin J. T., Davis S. N., and Elmore D. (1987) Applications of ^{129}I and ^{36}Cl in hydrology. *Nucl. Inst. Meth. Phys. Res. B* **29,** 361–371.

Feige Y., Oltman B. G., and Kastner J. (1968) Production rates of neutrons in soils due to natural radioactivity. *J. Geophys. Res.* **73,** 3135–3142.

Fisher Q. J. and Wignall P. B. (2001) Palaeoenvironmental controls on the uranium distribution in an Upper Carboniferous black shale (*Gastrioceras listeri* marine band) and associated strata; England. *Chem. Geol.* **175,** 605–621.

Friedman S. A. (1989) *Geology and Coal Deposits of the Clinton Area, West-Central Indiana*. Geological Survey Special Report 42. Indiana Department of Natural Resources.

Gladney E. S., Peters R. J., and Eberhart W. (1991) Radium-226 in geologicals—Gamma-ray spectrometry. In *Health and Environmental Chemistry: Analytical Techniques, Data Management, and Quality Assurance*, Vol. I (eds. M. A. Gautier and E. S. Gladney), pp. ER170-1–ER170-5. Los Alamos National Laboratory, Los Alamos, NM.

Gosse J. C. and Phillips F. M. (2001) Terrestrial in situ cosmogenic nuclides: Theory and application. *Quat. Sci. Rev.* **20,** 1475–1560.

Gray H. H., Ault C. H., and Keller S. J. (1987) Bedrock geologic map of Indiana. Indiana State Geological Survey Miscellaneous Map 48.

Harwood R. J. (1977) Oil and gas generation by laboratory pyrolysis of kerogen. *AAPG Bull.* **61**(12), 2082–2102.

Heaton R., Lee H., Skensved P., and Robertson B. C. (1989) Neutron production from thick-target (α,n) reactions. *Nucl. Inst. Meth. Phys. Res. A* **276,** 529–538.

Hover V. C., Peacor D. R., and Walter L. M. (1996) Relationship between organic matter and authigenic illite/smectite in Devonian black shales, Michigan and Illinois Basins, USA. In *Siliciclastic Diagenesis and Fluid Flow: Concepts and Applications*, Special Publication 55, pp. 73–83. Society for Sedimentary Geology, Tulsa, OK.

Kaplan I. (1963) *Nuclear Physics*. 2nd ed. Addison-Wesley, Reading, PA.

Klemme H. D. and Ulmishek G. F. (1991) Effective petroleum source rocks of the world: Stratigraphic distribution and controlling depositional factors. *AAPG Bull.* **75**(12), 1809–1851.

Krauskopf K. (1979) *Introduction to Geochemistry*. 2nd ed. McGraw-Hill, New York.

Lehmann B. E., Loosli H. H., and Pearson F. J. Jr. (1990) Limit to the use of ^{4}He and ^{36}Cl for groundwater dating. In *Memoires, International Conference on Water Resources in Mountainous Regions, Lausanne 22 Pt 1* (ed. A. Parriaux), pp. 357–363. International Association of Hydrogeologists, Kenilworth, UK.

Leininger R. K. (1981) Inorganic geochemistry. In *Studies of the New Albany Shale (Devonian and Mississippian) and Equivalent Strata in Indiana* (eds. N. R. Hasenmueller and G. S. Woodward), pp. 53–61. Indiana Department of Natural Resources, Geological Survey.

Lev S. M., McLennan S. M., Meyers W. J., and Hanson G. N. (1998) A petrographic approach for evaluating trace-element mobility in a black shale. *J. Sediment. Res.* **68**(5), 970–980.

Lev S. M., McLennan S. M., and Hanson G. N. (1999) Mineralogic controls on REE mobility during black-shale diagenesis. *J. Sediment. Res.* **69**(5), 1071–1082.

Lev S. M., McLennan S. M., and Hanson G. N. (2000) Late diagenetic redistribution of uranium and disturbance of the U-Pb whole rock isotope system in a black shale. *J. Sediment. Res.* **70**(5), 1234–1245.

Leventhal J. S. and Kepferle R. C. (1982) Geochemistry and geology of strategic metals and uranium in Devonian shales of the eastern interior United States. In *Synthetic Fuels From Oil Shale II, Nashville*, pp. 73–96. Institute of Gas Technology, Chicago.

Liu B., Phillips F. M., Fabryka-Martin J. T., Fowler M. M., and Stone W. D. (1994) Cosmogenic ^{36}Cl accumulation in unstable landforms, 1. Effects of the thermal neutron distribution. *Water Resour. Res.* **30,** 3115–3125.

Liverhant S. E. (1960) *Elementary Introduction to Nuclear Reactor Physics*. John Wiley, New York.

Martel D. J., O'Nions R. K., Hilton D. R., and Oxburgh E. R. (1990) The role of element distribution in production and release of radiogenic helium: The Carnmenellis Granite, southwest England. *Chem. Geol.* **88,** 207–221.

McGowan C., Leimer H. W., and Kerr C. P. (1983) Characterization of organic material in Chattanooga oil shale and shale oil. In *Synthetic Fuels From Oil Shale and Tar Sands*, pp. 229–245. Institute of Gas Technology, Chicago.

Meinschein W. G. (1981) Organic geochemistry. In *Studies of the New Albany Shale (Devonian and Mississippian) and Equivalent Strata in Indiana* (eds. N. R. Hasenmueller and G. S. Woodward), pp. 45–52. Indiana Department of Natural Resources, Geological Survey.

Meunier J. D., Landais P., and Pagel M. (1990) Experimental evidence of uraninite formation from diagenesis of uranium-rich organic matter. *Geochim. Cosmochim. Acta* **54,** 809–817.

Moore G. W. (1954) Extraction of uranium from aqueous solution by coal and some other materials. *Econ. Geol.* **49,** 652–658.

Mughabghab S. F., Divadeenam M., and Holden N. E. (1981) *Neutron Cross Sections, Volume 1, Neutron Resonance Parameters and Thermal Cross Sections, Part A, Z = 1-60*. Academic Press, Orlando, FL.

Nakashima S., Disnar J. R., Perruchot A., and Trichet J. (1984) Experimental study of mechanism of fixation and reduction of uranium by sedimentary organic matter under diagenetic or hydrothermal conditions. *Geochim. Cosmochim. Acta* **48,** 2321–2329.

Nolte E., Krauthan P., Korschinek G., Maloszewski P., Fritz P., and Wolf M. (1991) Measurements and interpretations of ^{36}Cl in groundwater, Milk River aquifer, Alberta, Canada. *Appl. Geochem.* **6,** 435–445.

Parrington J. R., Knox H. D., Breneman S. L., Baum E. M., and Feiner F. (1996) *Nuclides and Isotopes*. 15th ed. General Electric Co. and KAPL Inc.

Phillips F. M. (2000) Chlorine-36. In *Environmental Tracers in Subsurface Hydrology* (eds. P. G. Cook and A. L. Herczeg), pp. 299–348. Kluwer, Boston.

Phillips F. M., Bentley H. W., Davis S. N., Elmore D., and Swanick G. B. (1986) Chlorine 36 dating of very old groundwater 2. Milk River Aquifer, Alberta, Canada. *Water Resour. Res.* **22**(13), 2003–2016.

Phillips F. M., Stone W. D., and Fabryka-Martin J. T. (2001) An improved approach to calculating low-energy cosmic-ray neutron fluxes near the land/atmosphere interface. *Chem. Geol.* **175,** 689–701.

Purser K. H., Elmore D., Mueller K. A., Miller T. E., Hyder H. R. M., and Enge H. (1994) Upgrading program for the FN tandem and AMS system at PRIME Lab. *Nucl. Inst. Meth. Phys. Res. B* **92,** 69–73.

Shanbhag P. M. and Choppin G. R. (1981) Binding of uranyl by humic acid. *J. Inorg. Nucl. Chem.* **43**(12), 3369–3372.

Stephenson R. (1954) *Introduction to Nuclear Engineering*. McGraw-Hill, New York.

Stone J. O. H., Evans J. M., Fifield L. K., Allan G. L., and Cresswell R. G. (1998) Cosmogenic chlorine-36 production in calcite by muons. *Geochim. Cosmochim. Acta* **62,** 433–454.

Szalay A. (1964) Cation exchange properties of humic acids and their importance in the geochemical enrichment of UO_2^{++} and other cations. *Geochim. Cosmochim. Acta* **28,** 1605–1614.

Tissot B. P. and Welte D. H. (1978) *Petroleum Formation and Occurrence: A New Approach to Oil and Gas Exploration*. Springer-Verlag, Berlin, Germany.

Tourtelot H. A. (1979) Black shale—Its deposition and diagenesis. *Clays Clay Min.* **27**(5), 313–321.

Vinogradov A. P. (1962) Average contents of chemical elements in the principal types of igneous rocks of the earth's crust. *Geochemistry* **7,** 641–664.

Vogt S., Elmore D., and Fritz S. J. (1994) ^{36}Cl in shallow, perched aquifers from central Indiana. *Nucl. Inst. Meth. Phys. Res. B* **92,** 398–403.

Williams M. M. R. (1966) *The Slowing Down and Thermalization of Neutrons*. Elsevier, New York.

Woosley S. E., Fowler W. A., Holmes J. A., and Zimmerman B. A. (1975) *Tables of Thermonuclear Reaction Rate Data for Intermediate Mass Nuclei*, OAP-422. California Institute of Technology, Pasadena.

Ziegler J. F. (1977) *The Stopping and Ranges of Ions in Matter, Vol. 4: Helium Stopping Powers and Ranges in All Elemental Matter*. Pergamon, New York.

Ziegler J. F., Biersack J. P., and Littmark U. (1985) *The Stopping and Range of Ions in Solids*. Pergamon, New York.

Zreda M. G., Phillips F. M., Elmore D., Kubik P. W., Sharma P., and Dorn R. I. (1991) Cosmogenic chlorine-36 production rates in terrestrial rocks. *Earth Planet. Sci. Lett.* **105,** 94–109.

APPENDIX

A.1. Calculation of the ^{36}Cl Ratio

The neutron production rate (P_n) due both to (α,n) reactions and spontaneous fission, and expressed as neutrons per gram of rock per year, is calculated from

$$P_n = {}^{238}N\lambda_{sf}\nu + a[\mathrm{U}] + b[\mathrm{Th}], \tag{A1}$$

where ^{238}N is the number of ^{238}U atoms per gram of rock, λ_{sf} is the spontaneous fission decay constant for ^{238}U (8.5×10^{-17} yr^{-1}), ν is the average number of neutrons (2.2) emitted per spontaneous fission of ^{238}U, and [U] and [Th] are the uranium and thorium concentrations (in ppm) for the rock matrix (Andrews et al., 1989). Using the atomic weight of ^{238}U (238.050785 amu) and the present atomic fraction of ^{238}U (0.992745) (Parrington et al., 1996), Eqn. A1 becomes

$$P_n = 0.470[\mathrm{U}] + a[\mathrm{U}] + b[\mathrm{Th}]. \tag{A2}$$

The coefficients a and b in Eqns. A1 and A2 give the neutron yield related to the light element composition of the matrix (in neutrons per gram of rock per year per ppm U or Th) and are calculated from the following relationships:

$$a = \frac{\sum_i S_i F_i Y_i^{\mathrm{U}}}{\sum_i S_i F_i} \tag{A3}$$

and

$$b = \frac{\sum_i S_i F_i Y_i^{\mathrm{Th}}}{\sum_i S_i F_i}, \tag{A4}$$

where S_i is the mass stopping power of element i (in MeV cm^2 g$_i^{-1}$) for an α particle of some chosen energy (MeV), F_i is the fractional abundance for element i, and Y_i^{U} and Y_i^{Th} are the neutron yields for element i per part per million of U and Th in equilibrium with their daughter products (Andrews et al., 1986). The mass stopping power (S_i) of an element depends on the energy of the incident α particle and is represented by

$$S = -\frac{\mathrm{d}E}{\rho \mathrm{d}x}, \tag{A5}$$

where ρ is the density of the medium and dE is the energy lost by the charged particle as it travels through a distance dx. With an average α energy for the natural decay chains of 5.51 MeV and with the stopping power tables of Ziegler (1977) tabulated in increments of 1 MeV, the reasonable choice for the energy of the mass stopping power in Eqns. A3 and A4 is to round up to 6 MeV. The neutron yields Y_i^{U} and Y_i^{Th} are included in Table 6.

The neutron flux (in units of neutrons per cm^2 per year) is defined by the following equation, including the thermal component in the first term and the epithermal component in the second term:

$$\Phi_n = p(E)\frac{P_n}{\Sigma_a} + [1 - p(E)]\frac{P_n}{I'_{\mathrm{eff}}}. \tag{A6}$$

Φ_n represents the total neutron flux (in neutrons cm^{-2} yr^{-1}), $p(E)$ is the resonance escape probability for a neutron to reach thermal energy and thus $[1 - p(E)]$ represents the probability that a neutron will be

absorbed in the epithermal energy region, P_n is the total rate of neutron production (in neutrons per gram of rock per year), Σ_a is the macro thermal neutron absorbance cross section of the rock (in cm^2 per gram of rock), and I_{eff} is the effective resonance integral for the rock (in cm^2 per gram of rock). The effective resonance integral is defined by (Williams, 1966)

$$I_{eff} = \sum_i I_i, \tag{A7}$$

where I_i is the resonance integral for element i (in cm^2 per atom). Resonance integrals are tabulated in references such as the chart of the nuclides (Parrington et al., 1996) and *Neutron Cross Sections* (Mughabghab et al., 1981). Eqn. A7 is more useful in the form

$$I'_{eff} = \sum_i N_i I_i, \tag{A8}$$

where N_i is the atomic density of element i in atoms per gram of rock. The resonance escape probability $p(E)$ is the probability that a free neutron will escape absorption as it travels between energies E_o and E (Liverhant, 1960), the range of the epithermal neutron region. The resonance escape probability is a function of the absorption probability of neutrons in the epithermal region, P_a (Liverhant, 1960),

$$p(E) = \exp(-P_a) \tag{A9}$$

and can be calculated from (Williams, 1966)

$$p(E) = \exp\left[-\frac{N_i}{\xi_i \Sigma_s} I_{eff}\right], \tag{A10}$$

where ξ_i represents the average logarithmic energy loss of a neutron per collision with target element i. Σ_s is the macro scattering cross section of the element (in cm^2 per gram of rock), which is calculated by

$$\Sigma_s = \sum_i N_i \sigma_{s,i}, \tag{A11}$$

where $\sigma_{s,i}$ is the scattering cross section of element i (cm^2). Similar in form to Eqn. A11, the macro absorption cross section of an element can be calculated by

$$\Sigma_a = \sum_i N_i \sigma_{a,i}, \tag{A12}$$

where $\sigma_{a,i}$ is the absorbance cross section of element i (cm^2). Cross sections are typically reported in the literature in units of barns, where 1 barn is equal to 10^{-24} cm^2. For use in the formulas, these cross sections are typically converted to square centimeters. Eqn. A10 thus becomes

$$p(E) = \exp\left[-\frac{I'_{eff}}{\sum_i \xi_i N_i \sigma_{s,i}}\right]. \tag{A13}$$

The average logarithmic energy loss per collision, ξ_i, is defined as 1 for hydrogen and for other elements can be calculated from (Kaplan, 1963)

$$\xi_i = 1 + \frac{r_i}{1 - r_i} \ln r_i, \tag{A14}$$

where r_i represents the maximum energy that can be lost by the neutron in a single collision with target i in a medium of mass number A. This parameter is calculated by

$$r_i = \left[\frac{A_i - 1}{A_i + 1}\right]^2, \tag{A15}$$

where A_i is the mass of element i (Kaplan, 1963).

Using the total neutron flux calculated from Eqn. 6, the ^{36}Cl ratio ($^{36}Cl/Cl$) for a rock in which the radioactive elements are in equilibrium with their daughter nuclides can be calculated from

$$R_{eq} = \Phi_{n(th)} \frac{1}{\lambda_{36} N_{Cl}} (\sigma_{35} N_{35} + \sigma_{39} N_{39}) + \Phi_{n(epi)} \frac{1}{\lambda_{36} N_{Cl}} (I_{35} N_{35} + I_{39} N_{39}), \tag{A16}$$

where $\Phi_{n(epi)}$ represents the thermal neutron flux (first term of Eqn. A6), $\Phi_{n(th)}$ represents the epithermal neutron flux (second term of Eqn. A6), λ_{36} is the decay constant for ^{36}Cl (2.30×10^{-6} yr^{-1}), σ_{35} is the thermal neutron absorption cross section for ^{35}Cl (43.6 barns/atom), I_{35} is the resonance integral for ^{35}Cl (18 barns/atom), σ_{39} is the thermal neutron absorption cross section for the $^{39}K(n,\alpha)^{36}Cl$ reaction (4.3 millibarns/atom), and I_{39} is the resonance integral for the same reaction (0.464 barns/atom). N_{39} is the number of ^{39}K atoms on an atom-per-gram-of-rock basis; using the atomic weight of potassium as 39.0983 g mol^{-1} and the atomic fraction of ^{39}K as 0.932581 (Parrington et al., 1996), $N_{39} = 1.44 \times 10^{16}$ [ppm K]. N_{35} and N_{Cl} represent the number of atoms of ^{35}Cl and the total number of atoms of stable chloride on an atom-per-gram-of-rock basis, respectively. Using the atomic weight of chlorine (35.4527 g mol^{-1}) and the atomic fraction of ^{35}Cl (0.7577 in Parrington et al., 1996), $N_{35} = 1.29 \times 10^{16}$ [ppm Cl] and $N_{Cl} = 1.70 \times 10^{16}$ [ppm Cl].

Making the appropriate substitutions, Eqn. A16 becomes

$$R_{eq} = p(E) \frac{P_n}{\Sigma_a} \frac{1}{[\text{ppm Cl}]} (1.44 \times 10^{-17} [\text{ppm Cl}] + 1.58 \times 10^{-21} [\text{ppm K}]) + [1 - p(E)] \frac{P_n}{I'_{eff}} \frac{1}{[\text{ppm Cl}]} \cdot (5.94 \times 10^{-18} [\text{ppm Cl}] + 1.71 \times 10^{-19} [\text{ppm K}]). \tag{A17}$$

It should be noted that parts per million Cl, residing in both numerator and denominator, can be cancelled out when assuming chemical homogeneity. But in a heterogeneous ratio calculation, doing so masks the differences between the chlorine available for neutron absorption in the numerator and the total chlorine in the denominator.

A.2. Calculation of Neutron Travel Distances

Neutron travel distances (as presented in Table 5) were calculated in the following manner. The elemental compositions given in Table 1 were further refined into separate nuclide concentrations for the light and intermediate elements up through sulfur using the nuclide abundances in Parrington et al. (1996). The isotopes of these elements have Coulomb barrier heights that allow (α,n) reactions to occur using the α particles emitted by the nuclides in the three natural decay chains. Concentrations of each stable nuclide were then used as a weighting factor applied to the maximum neutron emission energy after the reaction of the 8.78-MeV α particle of ^{212}Po with that nuclide. Polonium-212 emits the highest energy α particle of the three naturally occurring decay chains and therefore places an upper limit on the neutron emission energy. The maximum neutron emission energies were calculated using an algorithm presented in Beckurts and Wirtz (1964, p. 35). The summation of the weighted neutron emission energies represents the average maximum neutron emission energy for each shale sample. The fast-neutron path length was calculated using the transport mean free path and the log energy decrement. The transport mean free path (λ_{tr}) is the distance a neutron travels between collisions and is given by (Stephenson, 1954)

$$\lambda_{tr} = \frac{\lambda_s}{1 - \overline{\cos\psi}}, \tag{A18}$$

where λ_s is the scattering mean free path for the neutron and $\overline{\cos\psi}$ is the cosine of the average scattering angle for the neutron during interaction with moderator atoms. The scattering mean free path is the distance between scattering events for a neutron and is the reciprocal of the macro scattering cross section for the medium, Σ_s, calculated using Eqn. A11. The value of $\overline{\cos\psi}$ is calculated from (Stephenson, 1954)

$$\overline{\cos\psi} = \frac{2}{3A_i}, \tag{A19}$$

where A_i represents the average atomic mass of the particular moderator nuclei. The number of collisions (n) needed to moderate a neutron from an initial energy E_o to a final energy E is calculated using (Beckurts and Wirtz, 1964)

$$n = \frac{\ln(E_o/E)}{\xi}. \tag{A20}$$

The log energy decrement (ξ) for a homogeneous material is calculated using Eqns. A14 and A15, and the log energy decrement for a heterogeneous material is then calculated using

$$\xi = \frac{\sum_i N_i \xi_i}{\sum_i N_i}. \tag{A21}$$

By multiplying the transport mean free path (Eqn. A18), which represents the effective distance a neutron travels between collisions (Stephenson, 1954), by the average number of collisions needed to moderate the neutron from the initial average maximum energy to the final thermal energy of 0.0253 eV (Eqn. A20), one arrives at the fast-neutron path length. Path lengths for thermal neutrons can be calculated by assuming an average shale density of 2.4 g/cm^3 and inverting the macro absorption cross section, Σ_a, calculated using Eqn. A12. The total neutron travel length is the sum of the distances traveled at fast and thermal energies.

A.3. Calculation of α Particle Travel Distances

Alpha particle ranges (as presented in Table 5) were calculated by using the electron density of the rock as an inverse weighting factor. This is a consequence of the inverse relationship between the range of a charged particle traveling in a medium and the electron density of the medium (Balashov, 1997):

$$R_\alpha(E) \approx \frac{E^2}{m_a Z_a^2} \frac{1}{ZN}. \tag{A22}$$

Here, $R_\alpha(E)$ is the energy-dependent range of the α particle traveling in a medium of atomic number Z and atomic density N (and thus electron density ZN), E is the energy of the α particle, Z_a is the charge of the α particle, and m_a is the mass of the α particle. If the initial energy of an α particle is known, then the α range is an inverse function of electron density ZN only. The α particle range in heterogeneous media can be calculated using

$$\frac{1}{R_\alpha(E)} = \sum_i \left[\frac{Z_i N_i}{R_{\alpha,i}(E)} \frac{1}{\sum_i Z_i N_i} \right]. \tag{A23}$$

The form of the equation is from Fabryka-Martin (1988). The summation is performed over all elements and $R_{\alpha,i}(E)$ is the energy-dependant α range in element i. $R_{\alpha,i}(E)$ was determined by using the range formula of Ziegler (1977) to calculate α ranges in pure elemental media for each α-emitting nuclide in the three decay chains.